E-153

A Proposal for

MEASUREMENTS OF NUCLEON SPIN STRUCTURE AT SLAC IN END STATION A

Co-spokesmen: R. Arnold, J. McCarthy

R. Arnold, P. Bosted, J. Dunne, J. Fellbaum, S. Rock
Z. Szalata, J. White
American University, Washington D. C. 20016

A. Feltham, D. Fritschi, J. Jourdan, G. Masson
S. Robinson, I. Sick, P. Steiner
Institut für Physik der Universität, CH 4056 Basel, Switzerland

J. Gomez, J. Mitchell, S. Nanda
CEBAF, Newport News, VA 23606

P. Anthony, F. Dietrich
Lawrence Livermore National Laboratory, Livermore, CA 94550

A. Klein, S. Kuhn
Old Dominion University, Norfolk, VA 23529

J. Button-Shafer
University of Massachusetts, Amherst, MA 00013

T. Chupp
University of Michigan, Ann Arbor, MI 48109-1120

K. Griffioen, R. Antonov
University of Pennsylvania, Philadelphia, PA 19104

J. Clendenin, R. Gearhart, E. Hughes,
T. Maruyama, W. Meyer, A. Odian, G. Petratos,
R. Pitthan, C. Prescott, L. Rochester, L. M. Stuart
S. St. Lorant, H.Tang, T. Usher, K. Witte, C. Young
Stanford Linear Accelerator Center, Stanford University, Stanford, CA 94309

R. Erbacher, D. Kawall, Z. Meziani
Stanford University, Stanford, CA 94305

J. Xu
Syracuse University, Syracuse, NY 13210

K. Abe, F. Suekane, H. Yuta
Tohoku University

T. Averett, H. Baghaei, D. Crabb, D. Day, E. Friez, R. Gladyshev
S. Høibråten, R. Lindgren, T. Liu, R. Lourie, J. McCarthy, R. Minehart,
D. Pocanic, O. Rondon-Aramayo, C. Smith, S. VanVerst
University of Virginia, Charlottesville, VA 22901

H. Band, J. Johnson, R. Prepost, G. Zapalac
University of Wisconsin, Madison, WI 53706

ABSTRACT

This proposal is for a series of precision measurements of deep inelastic scattering of polarized electrons from polarized ammonia targets (NH3 and ND3) to determine the spin structure functions g_1 and g_2 of the proton and neutron over a range in Bjorken scaling variable $0.015 \leq x \leq 0.78$ and momentum transfer $1 \leq Q^2 \leq 13$ (Gev/c)^2. This will extend the range of precision spin structure measurements at low x, cutting the unmeasured region near $x = 0$ in half. This data will double the Q^2 range of precision measurements and allow a search for non-scaling higher-twist contributions to the spin structure functions. With careful attention to systematic errors, with measurements of contributions from g_2 in transverse asymmetries, and with measurements of possible higher-twist contributions, this data will allow precision tests of the sum rules for integrals over the g_1 structure functions. The Ellis-Jaffe sum rule $\int g_1^p(x)dx$ will be tested to $\pm 0.0017(\pm 0.0060)$ statistal (systematic) error, and the integral $\int g_1^n(x)dx$ will be tested to $\pm 0.0036(\pm 0.0074)$ statistical (systematic) error. The Bjorken sum rule $\int (g_1^p(x) - g_1^n(x))dx$ will be tested to $\pm 0.0047(\pm 0.0138)$ which is $\pm 3.2\%(\pm 9.3\%)$ if the sum is 0.148.

The measurements will be made in SLAC End Station A using a beam of polarized electrons at 48.55 GeV with polaraization $Pb \sim 0.8$. A new pair of focussing magnetic spectrometers instrumented with shower sounters and Čerenkov counters to measure scattered electrons and reject pions will be built. Six weeks of checkout and calibration with the A-line parasitic beam will be needed, and three calendar months of beam for data taking will be required.

The main request to SLAC is for approval: 1) to measure in End Station A with a 49 GeV beam; 2) to build the new spectrometer and detector systems described here; 3) to run for 6 weeks of checkout with the A beam in parasitic mode; and 4) to run for three calendar months for physics data.

INTRODUCTION

Measurements of the nucleon spin structure functions are necessary to provide fundamental tests of QCD and the quark structure of hadrons. Deep inelastic electron or muon scattering with polarized beams and polarized targets directly probes the distribution of the spin on the nucleon quark constituents. The data can be used to extract the proton and neutron spin structure functions, $g_1(x)$ and $g_2(x)$, for a direct test of quark models of nucleon structure. In addition the data can be used to test a number of sum rules based on various integrals of $g_1(x)$ and $g_2(x)$ over x, the Bjorken scaling variable. The most important of these is the Bjorken sum rule[1] which relates the integral of $g_1(x)$ for the proton and neutron to a number measured in neutron beta decay. The Bjorken sum rule is based on current algebra and a few fundamental principles at the root of QCD and the standard model. Bjorken has said "If the Bj sum rule is wrong then QCD is wrong." Therefore it must be tested.

Ellis and Jaffe have written two other sum rules[2] for the separate integrals over $g_1(x)$ of the proton and neutron that are also equal to some numbers measured in weak decays. The Ellis-Jaffe sum rules are derived with some model dependent assumptions, and therefore are less fundamental than the Bjorken sum rule. However they provide powerful constraints for testing nucleon structure.

In the past several years a new generation of experiments by SMC[3,4] at CERN and by E142[5] (and soon to be E143) at SLAC have provided (or will provide) new data that considerably extend the previous limited results from EMC[6] and SLAC[7,8] more than a decade ago. These new data offer the chance to see the spin distributions with some precision and enough kinematic coverage to begin effective tests of the sum rules. The evidence is not all in yet, with more data still to come from SMC and E143, but the experimental situation is far from satisfactory. The proton $g_1^p(x)$ measurements from EMC and earlier SLAC experiments disagree with the Ellis-Jaffe sum rule, and this can be interpreted as evidence that the spin in the proton is not carried by the quarks. These data have generated wide interest, and

a huge number of theoretical papers have been produced seeking to understand the result. Recent results from SMC using a deuteron target and E142 using a ^{3}He target give the first look at the neutron spin. The data indicate that $g_1^n(x)$ is small and negative at low x. Within the errors (large for SMC) the experiments are consistent. Using the SLAC-EMC proton data together with the Bjorken sum rule gives a prediction for $g_1^n(x)$ that is inconsistent with the E142 result.

Before we can say with confidence that the Bjorken sum rule is not satisfied, we clearly need more extensive and accurate data. Data with small errors are needed at low x to reduce the uncertainty from extrapolation of the sum rule integrals to $x = 0$. Any possible non-scaling behavior versus Q^2 must be ruled out, and the reliability of extracting the neutron spin structure from data on nuclear targets must be tested.

With the intense and highly polarized electron beam up to 50 GeV now available at SLAC, with improved spectrometer facilities in End Station A, and with the polarized targets now tested or under construction, it will be possible in the next few years to measure the spin structure functions with sufficient coverage in x and Q^2 and with errors small enough to test the sum rules to the level of 5% to 10%. The first step in that process will be the completion of experiment E143 next year using a polarized ammonia (proton and deuterated) to measure proton and neutron $g_1(x)$ and $g_2(x)$. E143 is optimized with spectrometer angles and detector configurations to measure in the range $0.03 \leq x \leq 0.7$ and $1 \leq Q^2 \leq 7$ (GeV/c)^2 using beam energies of 22 to 25 GeV.

A further step in the experimental program of spin structure functions at SLAC is presented in this proposal,which we refer to as E143-50 (E143 at 50 GeV). We propose to extend the measurements of proton and neutron spin beyond those to be done by E143 in three important areas:

1. by cutting the unmeasured region at low x in half and extending the measurements to slightly higher x,
2. by doubling the Q^2 range, and

3. by reducing the experimental errors.

The measurements we propose will cover the kinematic range $0.015 < x < 0.78$ and $1 < Q^2 < 13$ (GeV/c)^2 with small errors. Measurements with small errors are essential for testing the sum rules, especially at low x to reduce the error on the extrapolation to the unmeasured region in x.

Measurements over a range of Q^2 are necessary to test whether the spin structure functions obey scaling in the SLAC kinematic region. The Bjorken sum rule and Ellis-Jaffe sum rules require that scaling be valid. If it is discovered that the structure functions do not obey scaling and have a Q^2 dependence different from that expected from the normal QCD evolution plus target mass effects due to the presence of non-scaling higher twist terms, then the Q^2-dependent measurements will allow for corrections to be made so that the sum rules can be properly tested. The spin-averaged structure functions from unpolarized scattering show significant contributions from higher twist terms in the range $1 \leq Q^2 \leq 10$ (GeV/c)^2. Observation of non-scaling behavior of the spin structure functions would be important information needed for a complete understanding of the nucleon structure.

For the neutron we will always have the special problem of extracting reliable spin structure functions from scattering on polarized nuclear targets. We know from unpolarized scattering measurements that there are significant nuclear effects (generally referred to as the EMC effect) on the structure functions in the region $x \geq 0.2$ due to the distortion of the quark momenta from nuclear binding and for $x \leq 0.2$ from nuclear shadowing. Before we can say with confidence that we have extracted the spin structure appropriate for a free neutron we will have to demonstrate by measurements that we get the same results from different nuclear targets. Measurements of neutron spin structure with comparable accuracy from both deuterium and ^{3}He targets will be essential for this test.

To accomplish these goals we propose to make a number of changes to the experimental plan from those to be used by E143:

1. The beam energy will be raised to 48.55 GeV. This is the primary means for

extending the x and Q^2 range.

2. The spectrometers will be optimized in scattering angle and optics for maximum solid angle while maintaining adequate background rejection and resolution for measurements at 48.6 GeV.

3. A new detector system that identifies scattered electrons but avoids the large background of low energy particles and pions will be assembled. It will employ only Čerenkov counters and lead glass shower counters with no tracking detectors. The tracking will be effectively performed by the focussing properties of the new spectrometers.

While we are convinced that the resources required for this experiment in beam time, spectrometers, and equipment are worth the investment, we are also aware that SLAC has limited resources and that our plans must be economical. Therefore the plan in this proposal has been made with the following considerations in mind:

1. The spectrometers and detector systems have been designed to be used also by proposed experiment E149 with minimal changes. The spectrometers in this proposal as the same as those for E149 run at 49 GeV. The difference between E149 run at 29 GeV and this proposal is that one spectrometer must be repositioned in angle and detectors relocated.

2. The spectrometer and detector packages make extensive use of existing equipment. The major items (magnets, shielding, Čerenkov tanks, most of the lead glass) all exist at SLAC. The new equipment required (mostly phototubes) would be shared with E149 and with an extension of E142 to 50 GeV.

3. The spectrometer and detector systems are compatible with measurements of the neutron spin structure using the E142 style polarized ^{3}He target. It is expected that at some future date the E142 collaboration will propose to extend the measurements of $g_1^n(x)$ to lower x and higher Q^2 using the systems proposed here and the 48.6 GeV beam.

The following sections give more details on the physics and the experiment.

The main request to SLAC is for approval: 1) to measure in End Station A with a 49 GeV beam; 2) to build the new spectrometer and detector systems described here; 3) to run for 6 weeks of checkout with the A beam in parasitic mode; and 4) to run for three calendar months for physics data.

PHYSICS MOTIVATION

Definitions

In inclusive polarized-lepton scattering from polarized nucleons, the total deep-inelastic cross section can be split into symmetric and antisymmetric components. The symmetric part of the cross section is just the unpolarized cross section which in the laboratory frame is given by

$$\frac{d^2\sigma}{d\Omega dE'} = \sigma = \sigma_{Mott}\left[\frac{1}{\nu}F_2(\nu,Q^2) + \frac{2}{M}F_1(\nu,Q^2)\tan^2(\theta/2)\right]. \quad (1)$$

Here, $\nu = E - E'$, E and E' are the initial and final lepton energies, Ω is the detector solid angle, M is the nucleon mass, Q^2 is the four-momentum transfer squared, θ is the lepton scattering angle, $F_1(\nu,Q^2)$ and $F_2(\nu,Q^2)$ are the unpolarized structure functions, and $\sigma_{Mott} = 4\alpha^2 E'^2\cos^2(\theta/2)/Q^4$.

The antisymmetric part of the cross section is the embodiment of the nucleon spin structure functions, and its sign depends on the helicity of the nucleon relative to that of the incident lepton. The difference in cross sections with different helicity orientations[9,10] is sensitive to only the polarized part of the nucleon structure. For longitudinally polarized electrons and nucleons we have

$$\frac{d^2\sigma^{\uparrow\downarrow}}{d\Omega dE'} - \frac{d^2\sigma^{\uparrow\uparrow}}{d\Omega dE'} = \sigma^{\uparrow\downarrow} - \sigma^{\uparrow\uparrow} = \frac{4\alpha^2 E'}{Q^2 E}\Big[(E + E'\cos\theta)MG_1(\nu,Q^2) - Q^2 G_2(\nu,Q^2)\Big], \quad (2)$$

and for longitudinally polarized leptons and transversely polarized nucleons the result is

$$\frac{d^2\sigma^{\uparrow\leftarrow}}{d\Omega dE'} - \frac{d^2\sigma^{\downarrow\leftarrow}}{d\Omega dE'} = \sigma^{\uparrow\leftarrow} - \sigma^{\downarrow\leftarrow} = \frac{4\alpha^2 E'}{Q^2 E}E'\sin\theta\Big[MG_1(\nu,Q^2) + 2EG_2(\nu,Q^2)\Big], \quad (3)$$

where $G_1(Q^2,\nu)$ and $G_2(Q^2,\nu)$ are the spin structure functions. The sum of the

polarized cross sections is just twice the unpolarized cross section, $2\sigma = \sigma^{\uparrow\downarrow} + \sigma^{\uparrow\uparrow} = \sigma^{\uparrow\leftarrow} + \sigma^{\downarrow\leftarrow}$. In the asymptotic scaling limit the polarized and unpolarized structure functions are expressed in terms of a single variable, $x = Q^2/(2M\nu)$,

$$\begin{aligned} \lim_{Q^2,\nu\to\infty} M^2\nu G_1(\nu, Q^2) &= g_1(x), & \lim_{Q^2,\nu\to\infty} M\nu^2 G_2(\nu, Q^2) &= g_2(x), \\ \lim_{Q^2,\nu\to\infty} F_1(\nu, Q^2) &= F_1(x), & \lim_{Q^2,\nu\to\infty} F_2(\nu, Q^2) &= F_2(x). \end{aligned} \tag{4}$$

It can be shown from Equations (1-4) and the definition for the longitudinal asymmetry, $A^{\parallel} = (\sigma^{\uparrow\downarrow} - \sigma^{\uparrow\uparrow})/(2\sigma)$, that in the asymptotic limit,

$$g_1(x) - kg_2(x) = 2KA^{\parallel}\sigma/\sigma_{Mott}, \tag{5}$$

where the kinematical factors are defined by $K = EE'\cos^2(\theta/2)/[2x(E + E'\cos\theta)]$, and $k = 2xM/(E + E'\cos\theta)$. For $E = 49$ GeV $k < 0.02$ so $A^{\parallel}$ essentially measures g_1. Similarly for the the transverse asymmetry, $A^{\perp} = (\sigma^{\uparrow\leftarrow} - \sigma^{\downarrow\leftarrow})/(2\sigma)$,

$$g_1(x) + k'g_2(x) = 2K'A^{\perp}\sigma/\sigma_{Mott}, \tag{6}$$

where $K' = E\cos^2(\theta/2)/(2x\sin\theta)$, and $k' = 2E/(E - E')$. $A^{\perp}$ primarily measures g_2

It has been conventional in the past to express asymmetry measurements in terms of the virtual photon-nucleon asymmetries, $A_1(x)$ and $A_2(x)$. Expressions relating the A_1 and A_2 to the measured $A^{\parallel}$ and $A^{\perp}$ and kinematic factors containing $R = \sigma_L/\sigma_T$ are given in the Appendix. In the past it has also been necessary to neglect the contributions due to the A_2 because transverse asymmetries were not measured. In this proposal we follow Anselmino and Leader[11] and extract the structure functions $g_1(x)$ and $g_2(x)$ directly from measurements of $A^{\parallel}$, $A^{\perp}$ and σ using Equations (5) and (6).

Sum Rules

Theoretically, various sum rules have been established for various integrals over the proton and neutron spin g_1 structure functions. The Bjorken sum rule[1] is a QCD prediction derived from current algebra, and is given by the relation

$$\int (g_1^p - g_1^n)dx = \frac{1}{6}\frac{g_A}{g_V}(1 - \alpha_s(Q^2)/\pi), \tag{7}$$

where the ratio of the weak coupling constants found from beta decay measurements is $g_A/g_V = 1.254 \pm 0.006$, and the second term containing $\alpha_s(Q^2)$, the strong coupling constant, is the QCD correction for finite Q^2. For $\alpha_s(Q^2) = 0.27 \pm 0.02$ the Bjorken sum rule is predicted to be 0.191 ± 0.002.

The Ellis-Jaffe sum rules,[2] based on SU(3) symmetry, for the proton and neutron separately, and assuming that the nucleon does not contain polarized strange quarks, are given by[12]

$$\begin{aligned} \int g_1^p(x)dx &= \frac{1}{18}(9F - D)(1 - \alpha_s(Q^2)/\pi) = 0.174 \pm 0.018, \\ \int g_1^n(x)dx &= \frac{1}{18}(6F - 4D)(1 - \alpha_s(Q^2)/\pi) = -0.021 \pm 0.011, \end{aligned} \tag{8}$$

where $F = 0.47 \pm 0.04$ and $D = 0.81 \pm 0.03$ are weak coupling constants measured in beta decay. From Eq. (7)and Eq. (8) we get $F + D = g_A/g_V = 1.28$

The "transverse" structure function, g_2, has also been the focus of theoretical study over the years. Fundamentally $g_2(x)$ originates from the transverse motion and spin distributions of the quarks. The origin is similar to the processes which gives rise to σ_L in the spin-averaged structure functions. The function $g_2(x)$ is expected to be small compared to $g_1(x)$ and the contribution to $A^{\|}$ is reduced by kinematic factors. However measurements of $g_2(x)$ are essential to reduce the uncertainty in extracting $g_1(x)$ from $A^{\|}$.

Measurements of $g_2(x)$, even if they are of limited precision, are interesting in their own right for information on the transverse spin distributions. Sum rules for

g_2 have been developed by Burkhardt and Cottingham,[13] Wandzura and Wilczek,[14] and Belyaev and Ioffe.[15] Also, it has been suggested by the analyses of Leader and Anselmo[11] and Heimann[16] that there is a possible divergence of $g_2(x)$ at small x. This possiblility makes a measurement of g_2 especially appealing at small x. Recent studies by Jaffe and Ji[17] suggest that twist-3 contributions, reflecting quark-gluon interactions, are significant in $g_2(x)$, and that its measurement would be a unique opportunity to study them.

Q^2-Dependence

What about the Q^2 dependence of the spin structure functions? For a valid test of the sum rules the spin structure data must be in the scaling region. The QCD corrections to the sum rules due to the normal QCD evolution of the spin structure functions via the Alterelli-Parisi equations are expressed by $\alpha(Q^2)/\pi$ terms in Equations (7)and (8). Measurements made at different Q^2 need to be adjusted to some common Q^2 via the $\alpha(Q^2)/\pi$ correction before taking the integral over x. Since the spin-averaged functions F_1 and F_2 and the spin-difference functions g_1 and g_2 all depend on the same QCD operators and splitting functions, we expect the QCD evolution of g_1 and g_2 will have a similar shape to that for F_1 and F_2. We know from years of measurements of unpolarized scattering that F_1 and F_2 have significant Q^2 dependence. A recent analysis of SLAC electron and BCDMS muon data for F_2 by Virchaux and Milsztajn[18] is shown in Figure 1. Since the asymmetry $A_1 \simeq g_1/F_1 = g_1 2x(1+R)/F_2$, and if the Q^2 dependence of g_1, F_1, and F_2 comes only from QCD evolution, we would expect the asymmetry to be independendt of Q^2, and that would be the end of the story.

However, we also know from the Virchaux-Milsztajn analysis that F_2 has significant non-scaling contributions from higher twist. The dashed curve in Figure 1, containing only QCD plus kinematic target mass corrections, does not fit the data. They find the best fit, shown by the solid curve in Figure 1, when they fit the data to the form

$$F_2^{HT}(x_i, Q^2) = F_2^{LT}(x_i, Q^2)[1 + \frac{C_i}{Q^2}] \tag{9}$$

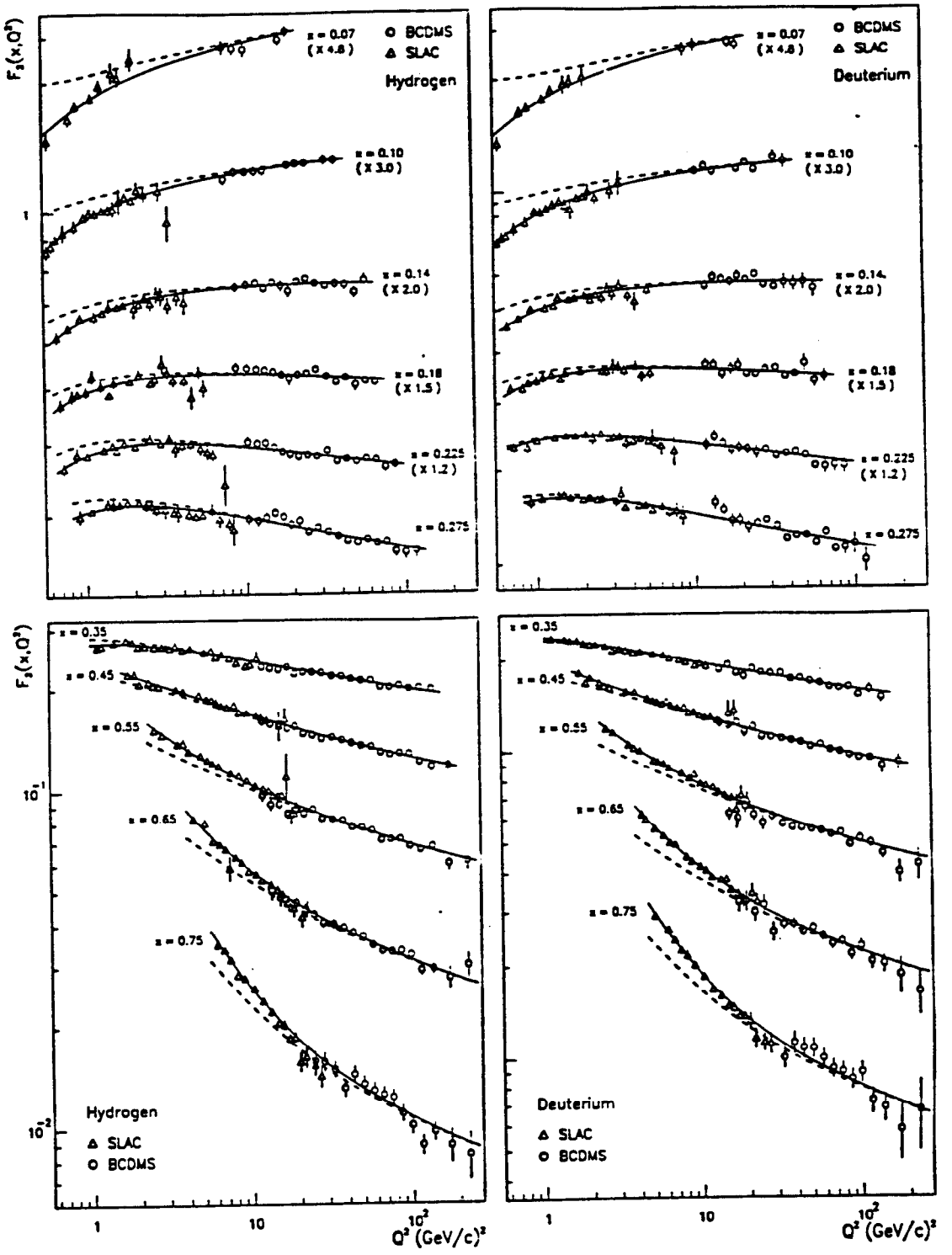

Fig 1. Next-to-leading order QCD fit to SLAC and BCDMS hydrogen and deuterium $F_2(x, Q^2)$ data with target mass corrections from Virchaux and Milsztajn [Ref (18)]. The solid line is the result of the full fit; the dashed line visualizes the Q^2 evolution without the twist-four corrections (leading-twist plus kinematic target mass corrections only).

where the C_i coefficients parametrize the presence of twist-four terms that fall with $1/Q^2$. The C_i values from the fits, shown in Figure 2, correspond to twist-four contributions to F_2 of 15% to 20% for Q^2 below 10 (GeV/c)^2.

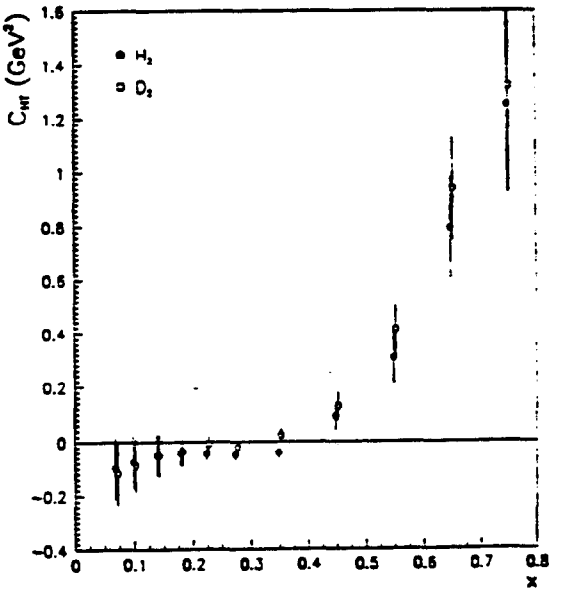

Fig. 2. The twist-four coefficients C_i as a function of x from Ref 18. Full (open) circles are for hydrogen (deuterium) data. The error in the C_i at low x is due to the uncertainty in the gluon structure function.

It is completely possible, even likely, that the spin structure functions, if examined closely enough, would also reveal non-scaling contributions at low Q^2. The origin of such terms, roughly speaking, corresponds to the virtual photon interacting with correlated quarks in the nucleon wave function (the diquark model is one extreme example). The scattering from such correlated quarks occurs with an extra penalty of $1/Q^2$ for finding the quarks in the correlated state. The spin structure functions of such correlations would not be the same as for single quarks. Two quarks can couple to either spin-zero or spin-one, which give different contributions to the $\sigma^{\uparrow\uparrow}$, $\sigma^{\uparrow\downarrow}$, $\sigma^{\uparrow\rightarrow}$ and $\sigma^{\uparrow\leftarrow}$. Therefore the spin structure functions might also be approximated with the form

$$g_1^{HT}(x_i, Q^2) = g_1^{LT}(x_i, Q^2)[1 + \frac{C_i^g}{Q^2}]. \qquad (10)$$

The coefficients C_i^g would not necessarily be the same as the C_i for the spin-averaged structure functions, and could possibly be larger. However, taking the

result of the Virchaux-Milsztajn fits as a guide, there could be twist-four contributions to the g_1 on the order of 15% to 20% for Q^2 below 10 (Gev/c)^2. Therefore when, as we propose, the spin structure functions g_1^p and g_1^d are measured with an accuracy of 5% to 8%, and especially when the Q^2 is below 10 (GeV/c)^2, we must look for the non-scaling contributions that might interfere with our interpretation of the sum rules. If such non-scaling terms can be observed, this information would be an important addition to our picture of nucleon structure.

If the higher-twist contributions are present and not accounted for, this would generate a systematic bias in the experimental test of the sum rules in experiments E142 and E143, which measure at $Q^2 < 10$ (GeV/c)^2. If the higher-twist contributions are as large as 10% to 15%, then lack of knowledge of the higher-twist corrections could be the largest source of systematic error.

SUMMARY AND COMPARISON OF PREVIOUS RESULTS

Measurements of the spin asymmetry, A_1^p, of the proton have been carried out at SLAC[7,8] and at CERN.[6] Future measurements are scheduled to be made at SLAC in experiment E143 and at CERN by the Spin Muon Collaboration (SMC).[3] Measurements of the neutron spin asymmetry, A_1^n, have been made by SLAC experiment E142[5] and measurements of the deuteron spin asymmetry, A_1^d, have been made by the SMC.[4] CERN has an advantage over SLAC in being able to make the measurements at higher beam energy (E = 100 to 200 GeV) and thus measure at higher Q^2 on the average, and can reach lower x while keeping $Q^2 > 1$ (GeV/c)^2. However the available counting rates at CERN are low and the errors from EMC and SMC results have been dominated by statistical errors. SLAC has the advantage over CERN of being able to make the measurements with significantly smaller errors, primarily due to much higher counting rates, but also due to better precision in some important parameters (beam polarization, random helicity flips on every pulse to eliminate false asymmetries from long term changes in counting rates, measurements of $A^\perp$).

Following is a summary of the experimental sum rule results which have been extracted from the asymmetry measurements. EMC[6] found that $\int g_1^p dx = 0.126 \pm 0.010 \pm 0.015$ which is in disagreement with the expected Ellis-Jaffe result given in Eq. (8). The first error is statistical and the second is systematic. SMC[4] found $\int g_1^d dx = 0.023 \pm 0.020 \pm 0.015$ and, using the EMC results, that $\int g_1^n dx = -0.08 \pm 0.04 \pm 0.04$ and $\int (g_1^p - g_1^n) dx = 0.20 \pm 0.05 \pm 0.04$. These results agree within errors with both the Ellis-Jaffe and Bjorken sum rule expectations. E142[5] has found, $\int g_1^n dx = -0.022 \pm 0.006 \pm 0.009$. This result together with the integral over the proton $g_1^p(x)$ from EMC gives the integral $\int (g_1^p - g_1^n) dx = 0.148 \pm 0.012 \pm 0.018$. This is to be compared to a Bjorken sum rule prediction of 0.187 ± 0.004, using $\alpha_s = 0.33 \pm 0.06$ for Q^2 between 2 and 10 $(\mathrm{GeV/c})^2$. The average Q^2 for the EMC data is 10.7 $(\mathrm{GeV/c})^2$, for the SMC data is 4.6 $(\mathrm{GeV/c})^2$, and for E142 is 2 $(\mathrm{GeV/c})^2$. The E142 and SMC results are consistent with each other within the errors (large for SMC).

The fact that the Bjorken sum rule appears to be violated is not good news for QCD. However, the disagreement is only 2σ, which could well be a fluctuation, and the systematic errors may have been underestimated. Given these results it is important to establish by independent experiments if there is a problem with the existing measurements, or if there are significant effects, such as from higher twist or nuclear dependence of the structure functions, that is interfering with the interpretation of the data. The E143 experiment and the one proposed here (E143-50) will address these issues.

EXPERIMENT GOALS AND POSSIBLE RESULTS

The goal of this proposal is to make precision measurements of the proton and neutron spin structure functions over the extended kinematic range available using a 48.6 GeV beam. The method used in this experiment is a direct extension of that to be used by E143. The principle features are:

1. Measurements of $A^{\parallel}$ and $A^{\perp}$ and σ for both proton (NH_3) and deuteron (ND_3) targets will be made. Values for $g_1^p(x)$, $g_2^p(x)$, $g_1^n(x)$, and $g_2^n(x)$ will be

extracted using Equations (5)and (6). The asymmetry $A^{\parallel}$ will be determined from the measured asymmetry $\Delta^{\parallel}$ defined in terms of the number of events N with a given orientation of the beam and target polarizations (parallel or opposite):

$$\Delta^{\parallel} = \frac{N^{\uparrow\downarrow} - N^{\uparrow\uparrow}}{N^{\uparrow\downarrow} + N^{\uparrow\uparrow}} = P_b P_t f(1 + C_{15}) A^{\parallel}, \qquad (11).$$

The statistical error on $A^{\parallel}$ is given by

$$\Delta A^{\parallel} = \frac{1}{\sqrt{N}} \frac{1}{P_b P_t f(1 + C_{15})} \qquad (12)$$

where $N = N^{\uparrow\downarrow} + N^{\uparrow\uparrow}$ is the total number of counts. The $A^{\perp}$ is given by a similar equation from measurements of the asymmetry $\Delta^{\perp}$ in $N^{\uparrow\leftarrow}$ and $N^{\downarrow\leftarrow}$ with opposite transverse target polarizations. The cross sections σ will be determined from a combination of measurements in this experiment for $x < 0.2$, and from normalization to the precision cross sections from E140,E140x for $x > 0.2$. The neutron asymmetries are extracted from measurements on the deuteron using

$$A_n = \left(1 + \frac{\sigma_p}{\sigma_n}\right) \frac{A_d}{\gamma} - \left(\frac{\sigma_p}{\sigma_n}\right) A_p \qquad (13)$$

where σ_p/σ_n is extracted from unpolarized deep inelastic scattering data on hydrogen and deuterium. The factor $\gamma \simeq 0.92$ is the effective polarization of the nucleons in the deuteron, discounting those in the D-state. These expressions depend on the polarization of the beam $P_b(\sim 0.8)$ and target free protons $P_t(\sim 0.9)$ and deuterons ($P_t \sim 0.4$) and on the dilution factor $f(\sim 0.12)$, which represents the ratio of the probability of scattering from a free proton or deuteron to the probability of scattering from all the nucleons in the target. The correction term C_{15} includes the effects of the nitrogen polarization in the ammonia molecule, and is of the order of 1.5%.

2. The x and Q^2 range will be extended by using a 48.6 GeV beam and a system of spectrometers and detectors optimized for that energy.

3. The experimental errors will be reduced as far as practical. The spectrometer, detector, and data acquisition systems have been designed to maximize the counting rates as far as possible within the constraints from the expected backgrounds. We also plan to make many checks and auxiliary measurements in a checkout run and in the main data run to calibrate the system and measure systematic effects and backgrounds.

The optimization of the spectrometers and detectors to achieve these goals is described in the next section. The parameters and assumptions used in the estimates of counting rates and experimental errors are given in the Appendix. The run plan to achieve these goals is given in the last section.

The possible results of this experiment and comparisons with other existing data are shown in Figures 3 through 7. The main results of this experiment will be:

1. Precision measurements (statistical errors roughly 1% to 2% per x bin for g_1^p and g_1^d) would be extended down to x of 0.015. This will cut in half the region at low x where precision cross sections are unmeasured by E142/E143, giving a corresponding reduction in the uncertainty from extrapolation of the sum rule integrals to $x = 0$.

2. The statistical errors on g_1^p will be a factor of 5 to 6 times smaller than those on the EMC measurements. The statistical errors on g_1^d will be a factor of 9 to 12 times smaller than those recently reported by SMC. The statistical errors on the extracted neutron g_1^n will be smaller by a factor of about 0.6 from those measured by E142.

3. For five or six x bins in the range $0.02 \leq x \leq 0.8$ there will be data of sufficient precision, together with data from E143 at lower Q^2, to measure the Q^2 dependence of A_1^p and A_1^d over roughly a factor of 2 to 3 range in Q^2 between $Q^2 = 1.5$ and 13 $(\mathrm{GeV/c})^2$. This is precisely the region where higher twist terms, if they exist, might be large enough to measure.

4. Measurements of $A^{\perp}$ will reduce the error from uncertainty in g_2 in the extraction of g_1 to negligible values. If g_2 turns out to be larger than some models suggest, but considerably smaller than the theoretical limit from $|A_2| \leq \sqrt{R}$, then it can be measured.

Table I gives a list of the sources and the expected values for the systematic errors of this experiment. Table II shows a comparison of estimates of the various sources of errors on the extracted integrals over the spin structure functions from the competing experiments.

Any extrapolation of the structure functions to the unmeasured regions is bound to be model dependent. The previous experiments have used various parameterizations to estimate the functions near the origin, usually based on a Regge shape. One can imagine that the functions remain well-behaved as x approaches zero. Then, with extrapolation based on reasonably straight lines toward the origin, the error on the extrapolation is directly proportional to the length of the extrapolation, and to the size of the error bars where the extrapolation begins. In our estimates we have made straight line extrapolations taking values at the upper and lower edge of the errors on the three lowest x data points, and computing the error on the extrapolation to be one half of the difference between the upper and lower error bars times the distance to the origin from the last data point. Of course the best way to constrain the extrapolation is to make measurements with small errors at the lowest possible x, which we propose to do. At high x the extrapolation error was estimated in a similar way, assuming that $g_1 \rightarrow 0$ as $x \rightarrow 1$. This contribution was small compared to the error from the low x extrapolation.

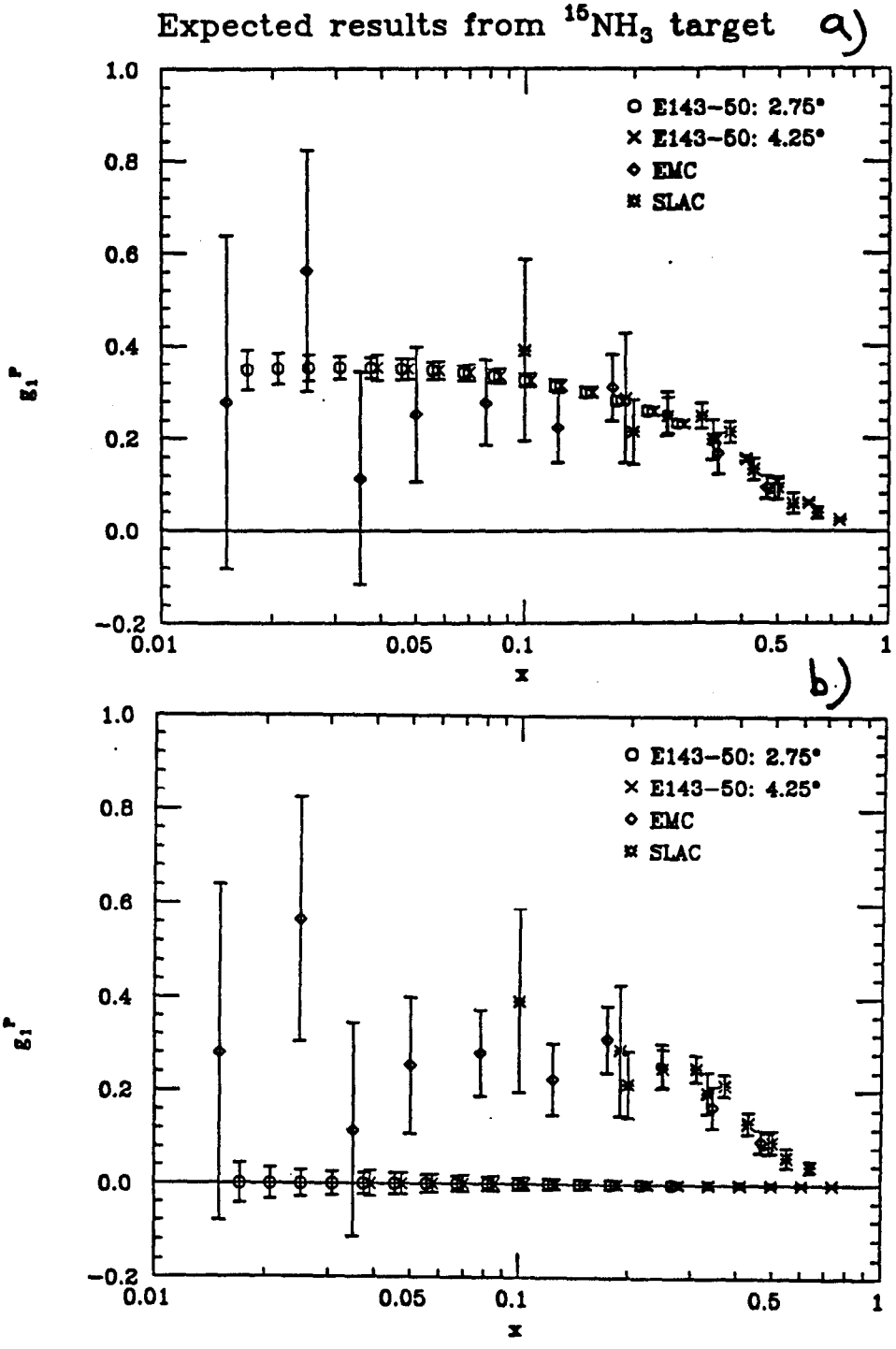

Fig. 3. Possible results from this experiment for $g_1^p(x)$. The error bars indicate the statistical errors for possible data in the 2.75° and the 4.25° spectrometers for 100 perfect hours of running at each of two spectrometer momentum settings. The previous data are from EMC (Ref. 6) and SLAC (Refs. 7, 8). Part a) shows possible results assuming the proton asymmetry model given in the Appendix. Part b) shows the size of our statistical errors assuming zero asymmetry so they can be distinguished from the other data points.

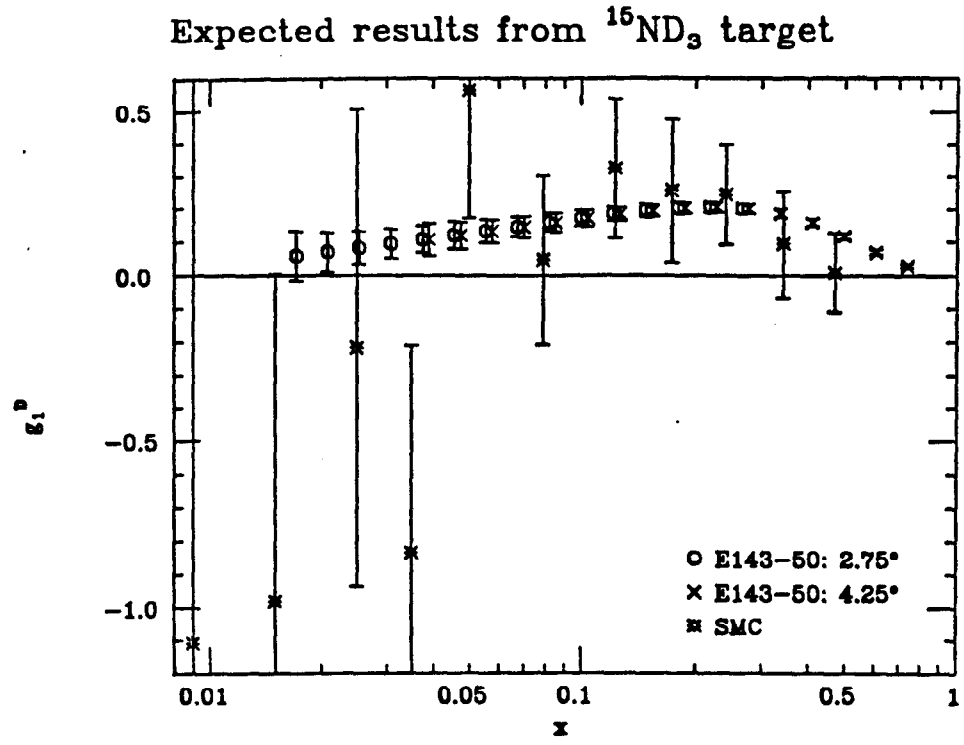

Fig. 4. Possible results from this experiment for g_1^d (statistical errors only). The values of g_1^d shown assume the fit to g_1^p shown in Fig. 3a and given in the Appendix that agrees with SLAC/EMC data and the fit to values of g_1^n from E142 shown in in Fig. 5 and also in the Appendix.

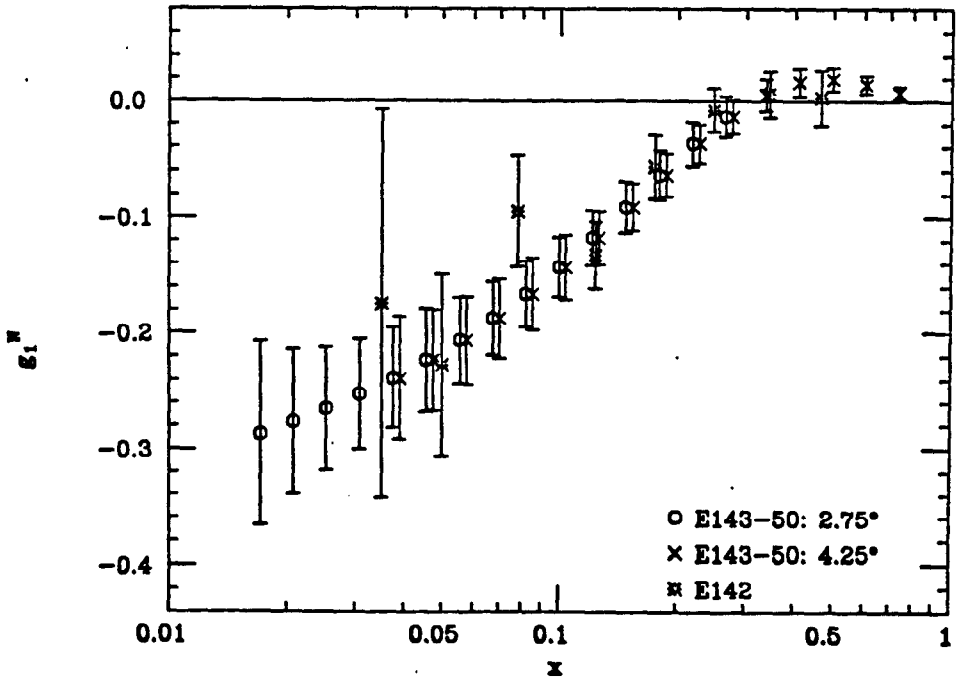

Fig. 5. Possible results from this experiment for g_1^n (statistical errors only) together with E142 data. The possible values for g_1^n are from a fit to the E142 data given in the Appendix.

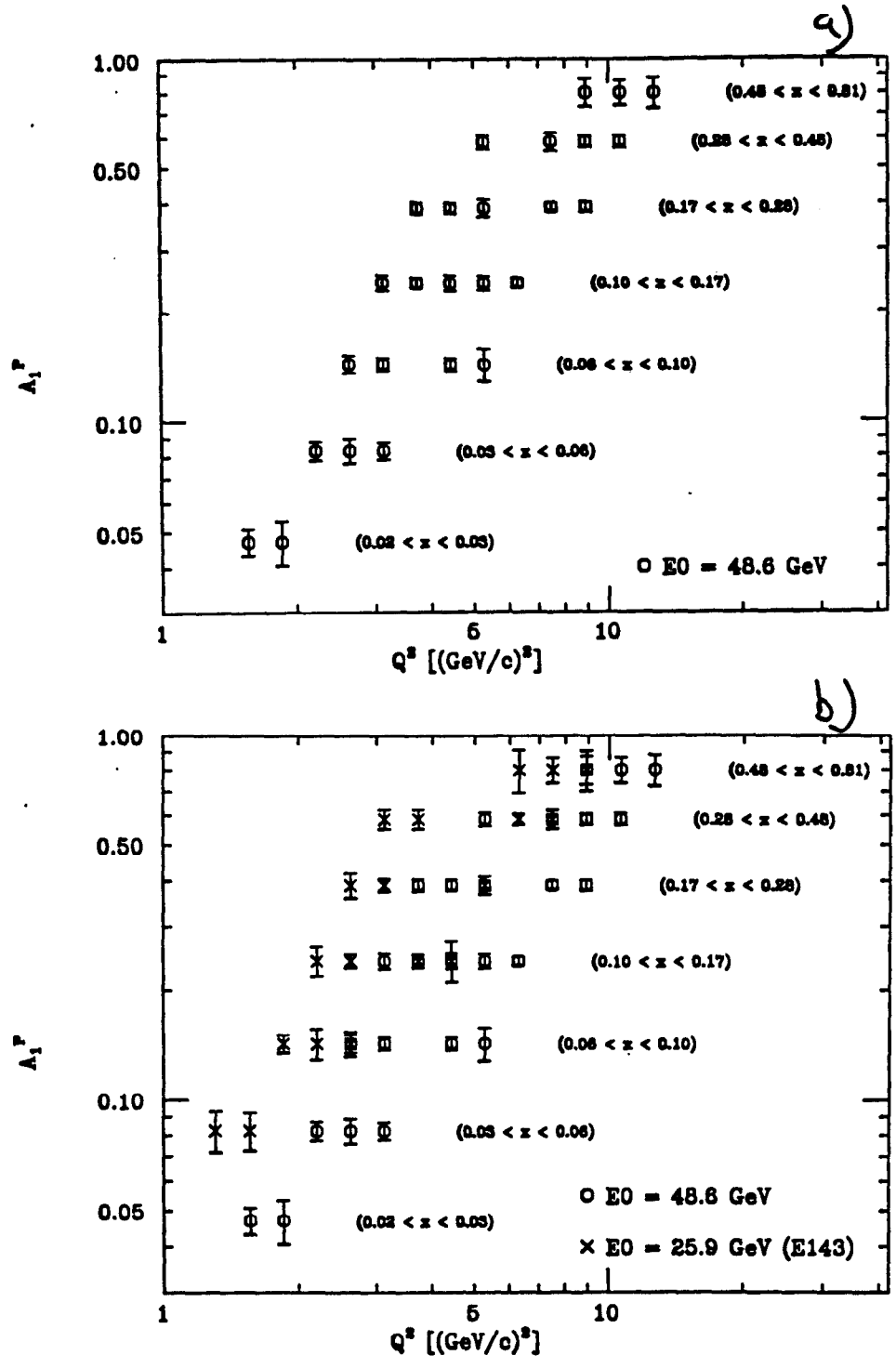

Fig. 6. Part a) possible results from this experiment for A_1^p versus Q^2 in bins of x (statistical errors only) assuming no deviations from the Q^2 dependence expected from QCD. Part b) Possible results from this experiment for A_1^p combined with expected results from E143. The combined data gives a larger range in Q^2 to look for higher twist contributions.

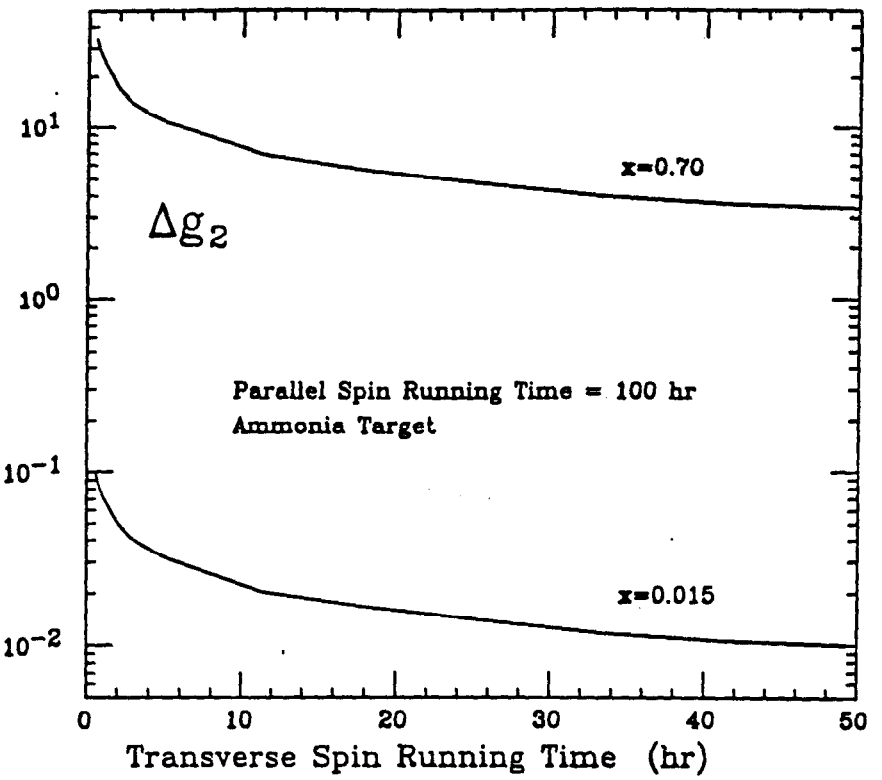

Fig. 7. Possible statistical errors for g_2^p in two x bins versus the required running time with transverse target polarization. The error for the extracted g_2 assumes the statistical error for the parallel spin running from 100 hours of data in each of two spectrometer settings. This curve helps us determine the transverse run time to be 20 hours per spectrometer setting. These resulting errors for g_2^p would reduce the uncertainty on the extracted g_1^p to negligible values due to the suppression of g_2^p in $A^{\|}$ by kinematical factors.

Table I
Sources of Systematic Error

Source	Factor	$x-$Range	Error	Error on g_1^p	Error on g_1^d
x-dependent errors					
Acceptance (for σ)	$\mathcal{A}$	$x < 0.2$	3%	1.2%	1.2%
(for normalization)		$x > 0.2$	1%		
Target length (for σ)	L	$x < 0.2$	2%	1.1%	1.1%
(for normalization)		$x > 0.2$	1%		
Kinematic factor	K	$x < 0.5$	1%	1%	1%
		$x > 0.5$	3%		
Dilution factor	f		2%	2%	2%
Nitrogen correction	C_{15}			0.1%	0.5%
Radiative correction	C_R	$x < 0.2$	5%	1.5%	1.5%
		$x > 0.2$	1%		
π, e^+ correction	C_π	$x < 0.05$	0.5%	0.2%	0.2%
		$x > 0.05$	0%		
Total x-dependent errors				3.1%	3.2%
x-independent errors					
Beam polarization	P_b			3%	3%
Target polarization	P_t			2%	5%
Beam charge	Q			0.1%	0.1%
Deuteron S State	γ				1.8%
Dead time,efficiency	C_{dt}			< 1%	< 1%
Total x-independent errors				3.7%	6.2%
Total systematic errors				4.8%	6.9%

TABLE II

Comparison of Errors for the Competing Spin structure Function Experiments
Error entries in the error table are in the form
statistical(% of sum)
systematic (% of sum)
extrapolation(% of sum)

	Sum	EMC+SLAC	SMC	E142	E143	E143-50
x_{min}		.01	.006	.03	.03	.015
x_{max}		.70	.60	.60	.70	.78
$\int g_1^p dx$	$.126^{+}$	.010(8.8%)			.0027(2.1%)	.0017(1.3%)
		.015(12%)			.0100(8%)	.0060(4.8%)
		.002(1.6%			.0023(1.8%)	.0010(0.8%)
$\int g_1^d dx$	$.100^{++}$		.020(87%)*		.0049(4.9%)	.0032(3.2%)
			.015(65%)*		.0110(11%)	.0069(6.9%)
			.005(21%)*		.0037(3.7%)	.0015(1.5%)
$\int g_1^n dx$	$-.022^{+++}$		.04(50%)**	.006(27%)	.0056(25%)	.0036(16%)
			.04(50%)**	.009(41%)	.0124(56%)	.0074(34%)
			? ?	.007(38%)	.0044(20%)	.0018(8.2%)
$\int(g_1^p - g_1^n)dx$	$.148^{++++}$		.050(25%)***	.012(8.1%)	.0073(4.9%)	.0047(3.2%)
			.040(20%)***	.018(12%)	.0230(15%)	.0138(9.3%)
			? ?	.007(4.7%)	.0059(4%)	.0025(1.7%)

Notes:

The errors for E143-50 take into acount that 5.3% of the errors on g_1^p and g_1^d are correlated, and assumes that the error from g_2^p and g_2^n is negligible.

$^{+}$ agrees with EMC+SLAC data.

$^{++}$ agrees with EMC+SLAC+E142 data.

$^{+++}$ areees with E142 data.

$^{++++}$ agrees with EMC+SLAC+E142 data but not with Bj sum rule prediction $\int(g_1^p - g_1^n)dx = 0.187$.

* percent errors of the sum $\int g_1^d dx = 0.023$ from SMC.

** percent errors of the sum $\int g_1^n dx = -0.08$ from SMC.

*** percent errors of the sum $\int(g_1^p - g_1^n)dx = 0.20$ from SMC.

The bottom line is that, barring large differences in the measured values of $g_1^p(x)$ and $g_1^n(x)$ from the ones assumed in these estimates, this experiment will reduce the errors on the sum rules from extrapolation of the integrals by a factor of 2.3 in the Bjorken sum rule from the expected E143 results and test the Bjorken sum rule to the level of 3% statistical error and 9% systematic error. This is accomplished primarily by extending the measurements to lower x, by reducing the statistical and systematic errors, by measuring the contribution from g_2, and by measuring or eliminating any contributions from higher-twist terms. These estimates assume that the functions are well behaved near $x = 0$. If nature turns out to have a different plan that gives some diabolical excursions of the spin structure functions at low x, then precision measurements at the lowest possible x will be essential for making a reliable extrapolation.

The projected improvements here in the statistical errors over those expected for E143 are due primarily to the increase by a factor of 3 in the solid angle of the new spectrometers. The decrease in cross section at fixed x with increasing Q^2 is nearly compensated by reducing the scattering angles.

Systematic Errors

In these estimates we have assumed that this experiment will be able to reduce some of the important systematic errors below the values assumed for E143. Partly this will be due to increased experience and understanding of our experimental equipment, and partly it will be due to the information gained in E143 that applies directly to some of the systematic uncertainties (measurements of the cross sections at low x and asymmetries at all x that are used in radiative corrections, for example). We will continue to work on reducing the systematic errors, and it is likely that experience with E143 will suggest a number of improvements to the techniques and operations that will reduce the errors further. An important result of the measurements versus Q^2 from this experiment and E143 is that we will be able to measure (or place limits on) the possible contributions from higher twist terms that could be contaminating the E143 (and E142) data. Contamination from higher twist, if it were present at the 10% to 15% level and not corrected, would

be the largest source of systematic error.

EXPERIMENTAL METHOD

The primary constraints which affected the experiment design were the following:

1. Kinematic coverage – We want to measure at the lowest x possible and still keep $Q^2 > 1$ (GeV/c)^2 to satisfy the requirement of being in the scaling region. We also want coverage in Q^2 over as large an x range as possible with reasonable counting rates to look for Q^2 dependence. To achieve both the x and Q^2 goals requires spectrometers at two different angles. With fixed beam energy, the $Q^2 > 1$ limit, together with the mechanical constraints from the sizes of magnets and the floor space in the End Station, determines the minimum usable scattering angle to be 2.75 degrees. At fixed beam energy it is primarily the decline in counting rate at large Q^2 and high x which determines the maximum useable scattering angle to be 4.25 degrees. Coverage at the high x end is also improved by going to higher beam energy because the limit of $W > 2$ GeV required to stay out of the resonance region can be met at higher x. There will also be some coverage at high x where $W < 2$ in the resonance region that will be useful. The kinematic coverage of this proposal compared with that for E142 and expected for E143 are shown in Figure 8.

2. Pion background – The pion rates are large at low x which is low E'. The π/e rates for a few kinematic conditions at 49 GeV are shown in Figure 9. Since the π/e rates decrease at fixed x with decreasing scattering angle, it is best to run at the smallest practical angle.

3. Radiative corrections – The radiative corrections increase at low E'. In general, we want to keep the potential error from uncertainty in the radiative corrections from being much larger than the other systematic errors, which total to about 8 % to 10 %. Our preliminary estimates for total radiative correc-

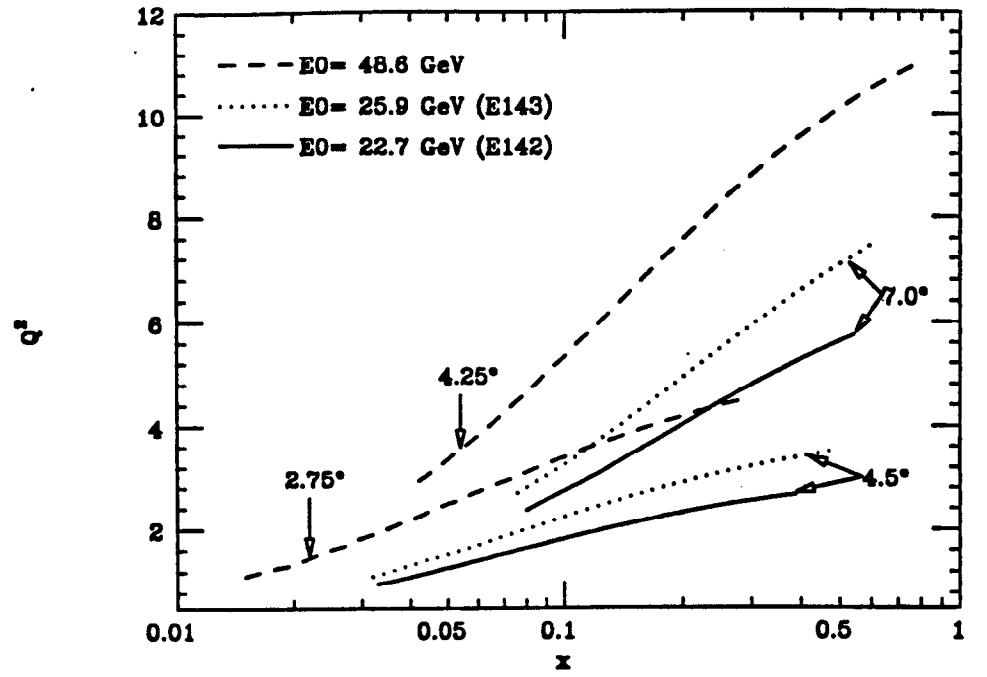

Fig. 8. The kinematic range in x and Q^2 of the proposed experiment, together with the range for E142 and projected for E143. The lines represent the center of the spectrometer acceptance at the indicated angles.

tion to the asymmetry for the proton, shown in Figure 10a, have a maximum value of 2 in the lowest x bin in each spectrometer ($A_{Raw}/A_{Born} = C_R \simeq 2$). The corresponding corrections on the spin-averaged cross sections, shown in Figure 10b , are about a factor of 3 in the lowest x bin. In previous experiments (E140, E140x) we have found that errors for radiative corrections to the unpolarized cross sections are about 1% as long as the corrections factors are $\leq$ 1.5. For the cross section measurements at low x the contributions from the elastic tail (known to 3% of its value) and inelastic tail (known to 3% of its value) are approximately equal to the Born cross sections. The α^4 and $\gamma - Z_0$ interference terms are less than 2%, and thus have small uncertainty. Therefore, the overall uncertainty to the extracted σ_{Born} due to radiative corrections in the lowest x bin is $\leq$ 5%. For the asymmetries, the uncertainty of the elastic form factors contributes an error of about 3%, and the error due to uncertainty on the inelastic is also about 3%. Thus the overall uncertainty in A_{Born} in the lowest x bin due to radiative corrections is about 5% of the value of the correction. As Figures 10a and 10b show, the

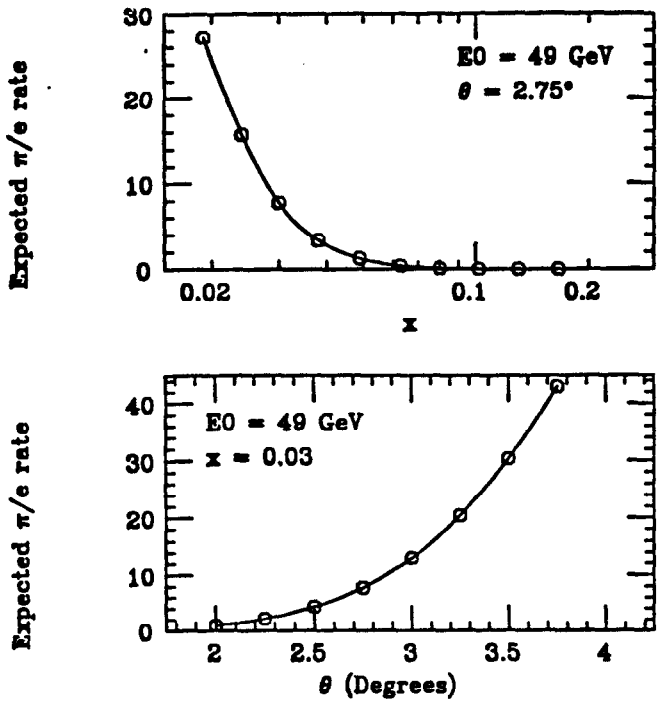

Fig. 9. The estimated π/electron rates at selected kinematics.

corrections, and thus the uncertainties, decrease rapidly with increasing x.

4. Spectrometer and detector design – The key problem for the spectrometer design is to get large acceptance for 10 to 40 GeV scattered electrons while maintaining high rejection of the pion flux, remaining insensitive to low energy spray background, and achieving the resolution in angle and energy needed to measure x and Q^2 with reasonable accuracy. The scheme we propose will use a focal plane system typical of spectrometers in the 1960's, before the invention of tracking chambers. To gain large acceptance, we will use shallow bend magnetic systems as close to the target and beam line as mechanical constraints will allow. With such a shallow bend, it is not feasible to make a double-bounce spectrometer required to operate detectors that measure ionization (scintillators or wire chambers). Therefore the traditional tracking detectors will not be used. Instead we use quadrupole focussing, to-

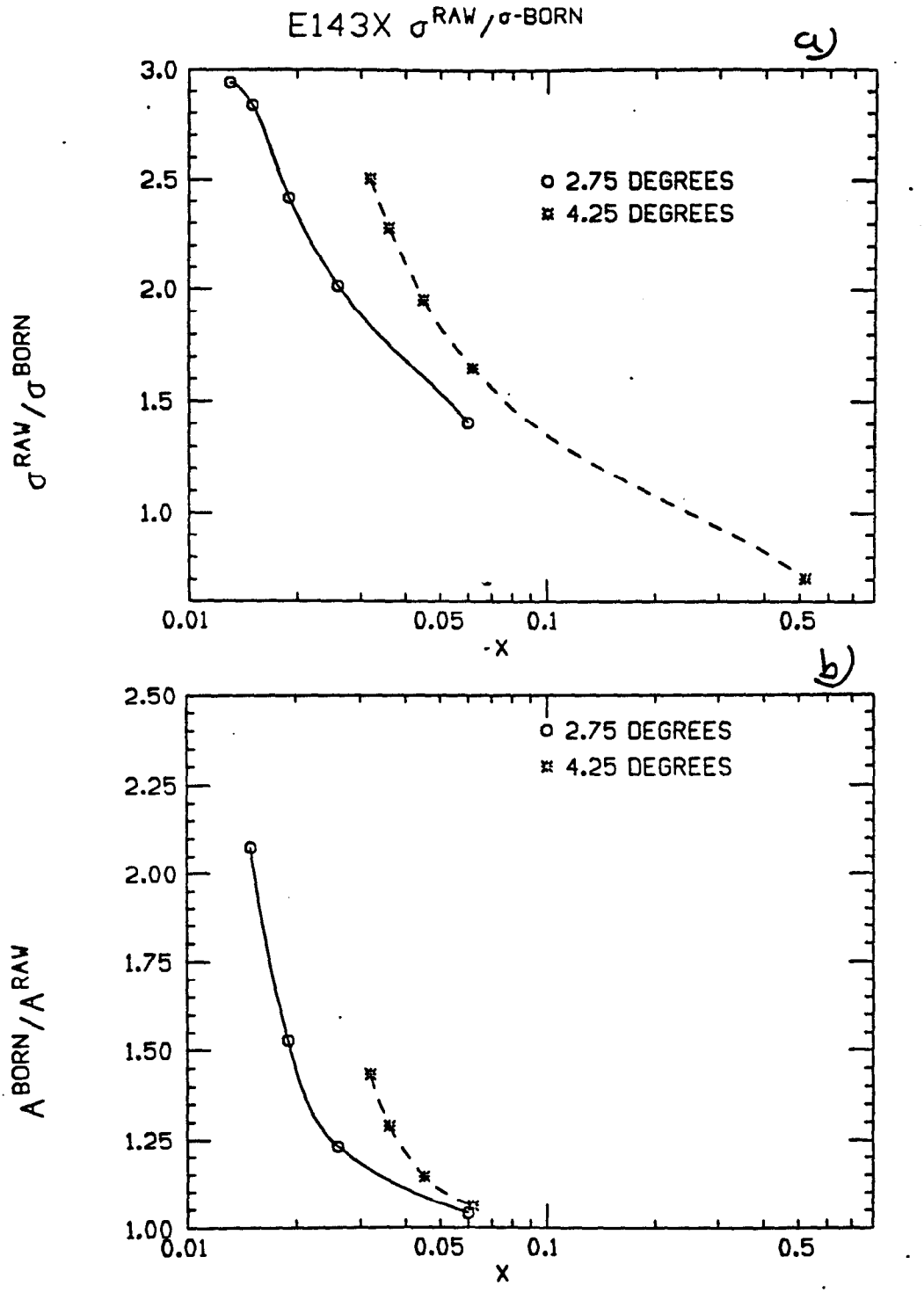

Fig. 10. Estimated radiative corrections for the proposed measurements. Part a) estimates of corrections to the cross sections, part b) estimates of corrections to the asymmetry $A^{\parallel}$ versus x at the kinematics corresponding to $E = 48.6$ GeV and the angles of the two spectrometers as shown.

gether with the bend, to deliver the particles to a tilted focal plane. Along the focal plane (or nearly so) will be a series of lead glass electromagnetic shower detectors. Lead glass detectors, which respond by the Čerenkov light in the glass, are relatively immune to low energy neutron and photon background. When the incoming momentum range of the particles is known from the spectrometer focussing, the blocks can give good discrimination of electrons from pions. To strengthen the pion rejection required at the lowest E', gas Čerenkov counters, operated at low pressures to give pion thresholds of 20 GeV, will also be used.

In the following sections we describe the proposed experiment in more detail.

Beam

Beam energy – We propose to measure mostly at a beam energy of 48.55 GeV using the SLED beam with 120 ns pulse length. This is the highest energy for spin precession of $N\pi$ in the A-line that can be achieved leaving sufficient spare klystrons for reliable accelerator operation. To deliver beam energy higher than 29 GeV into End Station A requires more bending power in the A-line. This can be achieved by adding existing magnets to the bend string. A plan for doing this has been under study for some time. For a small fraction of the data we plan to run at a lower energy (perhaps 25.9 GeV) to make cross section normalization measurements at the E143 kinematics.

Beam intensity – This experiment is limited to beam intensity around 2×10^9 electrons/pulse in a 120 ns SLED beam pulse to avoid heating and radiation damage to the polarized target. The actual beam intensities may be adjusted around this value for various tests and as experience establishes the actual limits of the target.

Polarization – For polarized beam we are assuming that beam with polarization of about 80% will be available from one of the strained lattice cathodes using the Ti-sapphire laser system now being tested for E143. The beam polarization will be flipped randomly on a pulse-to-pulse basis.

Beam rastering and control – Like E143, this experiment requires that the beam be rastered over the front surface of the target material to spread out the heat and radiation damage over the full target volume. We will require that the beam rastering and control system, now being upgraded for E143, be capable of rastering the 50 GeV beam over a target roughly 2 cm in diameter.

Parasitic beam – In addition to the main data run, we also request some time (6 weeks) using the parasitic electron beam in End Station A to check out and calibrate the spectrometers and detectors. The main job will be calibration of the response of the new shower counters to high energy electrons, and measurements of some of the optics properties and acceptances of the spectrometers. The shower counters will be calibrated by putting them directly in the beam at some convenient location upstream of the target.

The spectrometers can be calibrated using a low momentum test beam deflected into the spectrometers with simple magnetic systems at the target location. This would allow us to measure the important spectrometer matrix elements to verify the focal plane design and the acceptance by comparison with magnetic models. If this experiment is approved a more detailed plan for these tests will be presented.

Møller System

The beam polarization will be measured using single-arm and double-arm Møller scattering as in E143. It is possible that the Møller polarimeter will require little change for a beam energy of 50 GeV. The present Møller 18D72 spectrometer magnet will reach the momentum required to keep the Møller laboratory angle fixed to the nominal E142/E143 value of 7.77 mr. The Møller scatters then correspond to slightly backward hemisphere scattering at a CM angle of 120°, but this is in fact the kinematic condition used for the SLC Linac Møller polarimeter. The SLC Møller polarimeter has performed very well, and has comparable precision to the E142/E143 Møller polarimeter. There are, in fact, advantages to running Møller scattering under these kinematic conditions. While the analyzing power is somewhat smaller than at CM angle of 90° for E142/E143, this disadvantage is more than offset by the reduced background from the radiative tail from nuclear elastic scattering.

Consequently at this time we see no problem adapting the E142/E143 Møller polarimeter for a 50 GeV beam. After experience with E143 and reconsideration of the optimum scattering momentum and angle, we may elect to adjust the Møller spectrometer by adding another magnet or modifying the layout in some way.

If the Compton polarimeter proposed for E149 were operating at the time this experiment runs, then it would be desirable to use it. This could reduce the error from beam polarization, which is one of the larger systematic errors, from 3% to 1%.

Beamline in End Station A

The measurement of the $A^{\perp}$ asymmetries requires that the 5 Tesla target field be oriented perpendicular to the beam direction. As in E143, to compensate for the vertical deflection of the beam, a four-magnet chicane will be used. The field in the chicane magnets is adjusted to give the same $\int Bdl$ in each magnet equal to half of that for the target. The chicane is only turned on when the $A^{\perp}$ measurements are being made and it remains fixed in field at all energies. The spectrometer plan described below uses the same upstream chicane system of 10D37 magnets as E143, while the downstream 5D36 magnet pair is replaced with a single 10D37 magnet that will fit in the tight space constraints amid the spectrometer magnets.

The beamline down-stream of the target will be designed to gradually increase in diameter along its length to the back of the spectrometers, consistent with the constraints from the chicane and spectrometer magnets and shielding. The downstream beamline will contain some collimators and it will be closely integrated into the dense shielding between the spectrometers required to protect the detectors from target spray. As in E143 an SEM array will be used to measure beam profiles and the precision toroids will be used to measure beam currents.

Targets

The target for this proposal will be the same one used in E143. It consists of a 5 Tesla superconducting magnet, microwave systems for pumping the spins, NMR systems for measuring the polarization, and a cryostat and target refrigerator. This target uses irradiated frozen ammonia granules (NH_3) and deuterated (ND_3) cooled to $1K$. Under these conditions, ammonia has been shown[19][20] to have superior radiation resistance, allowing for high polarizations, luminosities of the order of $40 \times 10^{33} cm^{-2} s^{-1}$, and quick recovery of polarization losses. An open geometry superconducting Helmholtz coil provides the magnetic field to align the nuclei by the method of dynamic nuclear polarization.

We expect the E143 systems will be essentially useable without major changes, though experience may lead us to make some improvements. For the $A^{\parallel}$ and $A^{\perp}$ measurements we propose the target field will be oriented either parallel or perpendicular to the electron beam. The target stands, pipes, and other systems have been designed to allow a "quick" switch over by physically rotating the entire scattering chamber including the superconducting magnet in about one day.

We expect to achieve arget polarizations greater than 90% for protons and 40% for deuterons. At repetition rates of 120 pulses per second, the heat deposition in the target limits the beam currents to about 2×10^9 electrons per linac pulse.

Since the target is a key feature of this experiment, we give here an extended description of the principles of its operation and the status of the present developments for E143.

Solid Polarized Proton and Neutron Targets

Solid polarized targets work on the principle of Dynamic Nuclear Polarization in which a target material, eg. butanol, ethylene glycol, or ammonia, is doped, by chemical or radiation techniques, with a dilute assembly of paramagnetic atoms. The material is cooled to $\leq$ 1K in a magnetic field of a few Tesla and then irradiated by microwaves to drive the hyperfine transition which allows the nucleon(ar) spins to be aligned. All elements present in the material which possess a magnetic moment can be polarized at the same time. For spin-1/2 the polarization P is given by:

$$P = \tanh[\mu B/kT_s]$$

where μ is the magnetic moment, B is the magnetic field, k is Boltzman's constant and T_s is the spin temperature.

For many particle scattering experiments, the choice of a polarized target is dictated by the requirement that a basic figure of merit, F, of the type

$$F = P^2 I$$

be as large as possible. Here P is the polarization and I is the beam intensity. For example in the case where I is limited for some reason the choice would likely lead to a dilution refrigerator. Operation at very low temperatures would mean proton polarizations of greater than 90%.

However for this experiment the beam intensities are such that the material must be very resistant to radiation damage and must operate in a cryogenic environment which allows the most efficient removal of heat deposited by the beam. For these reasons the target material will be radiation-doped ammonia[21] (NH_3 and ND_3). The target system will be a ^{4}He evaporation refrigerator operating with a magnetic field of 5T. This is the same target to be used at SLAC for E143 during the Fall of 1993.

^{4}He is used because of its superior thermal properties compared to ^{3}He. Only 1K can be reached with ^{4}He so a 5T magnet is necessary to at least maintain the polarization which can be achieved by using ^{3}He at 0.5K in a field of 2.5T. Ammonia is the material of choice because of its resistance to radiation damage and its higher hydrogen or deuterium content compared to other materials.

Past experience at SLAC with a 5T/1K target[22] showed that operation with materials such as butanol doped with porphyrexide was limited by the radiation damage inflicted on the material. A large overhead in time was incurred because of the necessity to change the target at frequent intervals. Subsequently it was found, at Bonn,[23] at SLAC[19] and Michigan[24] under varying cryogenic conditions, that substantial polarizations could be obtained with radiation doped ammonia and that the radiation resistance was much better.

Development continued at Bonn, particularly with ND_3,[25] and at Michigan where it was found[20] that NH_3 could be quickly polarized to >90% in a 5T/1K system. At the AGS this target was used in a scattering experiment[26] using proton beams with intensities of up to 10^{11} protons/sec. Results relevant to this experiment are:

Radiation damage: The e^{-1} value for the initial fall of polarization with beam dose is 4×10^{15} protons/cm^2, a factor of ten better than the best chemically doped material. This is in very good agreement with the data of Seely et al.[27] from an electron beam at SLAC, and Althoff et al[28] from an electron beam at Bonn. After about 10^{15} protons pass through the target the radiation damage rate slows down giving an e^{-1} value of 1.3×10^{16} protons/cm^2. This is also in good agreement with the electron data.[27,28] In addition ammonia can be repeatedly annealed without loss of polarization, in contrast to chemically doped materials which have to be replaced after a few anneals.

Beam heating: With the ^{4}He cryostat used at the AGS a beam of 8×10^{10} protons/sec could be directed onto the target with a loss of only 2% in polarization. For a ^{3}He system a beam of 2×10^{10} protons/sec reduced the polarization by 15%.

Annealing: Generally the target was annealed when the polarization fell to about 80%. On the basis of the radiation damage values given in 1) a total of 3.25×10^{15} protons passes through the target while the polarization falls from 97% to 80%. For E143 running at 2.5×10^{11} electrons/sec this would mean annealing every 3.5 to 4 hours.

Polarization: The polarization is relatively insensitive to the bulk temperature. Even at 1.6K values of >70% were reached in 20 minutes.

Overall, an improvement of a factor of 12 in the figure of merit F, was achieved at the AGS by using this 5T/1K ^{4}He instead of the older 2.5T/0.5K ^{3}He target. There was also an increase in the operational efficiency. In comparison with the SLAC 5T/1K target used in previous experiments, with butanol as the target material, an increase in F of a factor of 10 should be obtained. We can also expect an increase in operational efficiency.

The radiation properties of ND_3 have been studied extensively by the Bonn group. Deuteron polarizations of about 50% have been obtained at 3.5T/0.3K with corresponding proton polarizations of about 100%. Measurements of ND_3 at 5T/1K, at SLAC, yielded polarizations of 25% but with proton polarizations of 75%, while recent measurements at Virginia yielded deuteron polarizations of 13% and proton polarizations of 95%. Under the same conditions as for NH_3, and with additional 'in-situ' (in ESA) irradiation, a deuteron polarization of 40% is expected. Work is continuing to improve the base deuteron value of 13%.

The disadvantage of using ammonia as a target is that the nitrogen is also polarized (up to about 20%). In the case of ^{14}N (spin 1) both the unpaired neutron and proton are polarized. But for ^{15}N (spin 1/2) there is only an unpaired proton to carry the polarization. The use of $^{15}ND_3$ and $^{15}NH_3$ as targets has several advantages the most important being a reduction in the systematic errors on the both the neutron and proton spin structure asymmetries. ^{15}N is commercially available at reasonable cost.

Status of the E143 Target – May 1993

5T Magnet – The magnet and cryostat were assembled and tested at the University of Virginia during the Fall of 1992. A drawing of the magnet is shown in Figure 11.

1K ^{4}He Refrigerator – The refrigerator design is such that it can be easily integrated into the magnet. A vertical target insert, moveable along the axis of the refrigerator will be used. It contains up to 4 target samples allowing easy positioning of the desired material in the beam.

NMR – A complete NMR system similar to the one used successfully at the University of Virginia during initial polarization studies is being assembled and tested at SLAC for E143. The system contains 5 'Liverpool' detectors allowing independent measurement of the different target material polarizations without re-tuning the system.

Ammonia targets – An apparatus has been set up to freeze ammonia and break it into fragments of appropriate size. $^{14}NH_3$, $^{14}ND_3$, and $^{15}NH_3$ have been produced in the form of 2.5 mm granules. The beads were irradiated both at CEBAF and at the Saskatoon Accelerator Laboratory (SAL) and were subsequently polarized at the University of Virginia.

The complete system was operated at the University of Virginia from August 1992 to February 1993 and, as noted above, proton polarizations of 95% and deuteron polarizations of 13% were obtained. Results are shown in Figure 12.

The system was shipped to SLAC in March 1993 and is currently being assembled and commissioned for E143. The magnet has already been operated at 5T at SLAC. In parallel, studies are being made with a view to increasing the base deuteron polarization before the 'in-situ' irradiation where, significant improvement is expected. Overall, proton polarizations of 90% and deuteron polarizations of 40% are expected.

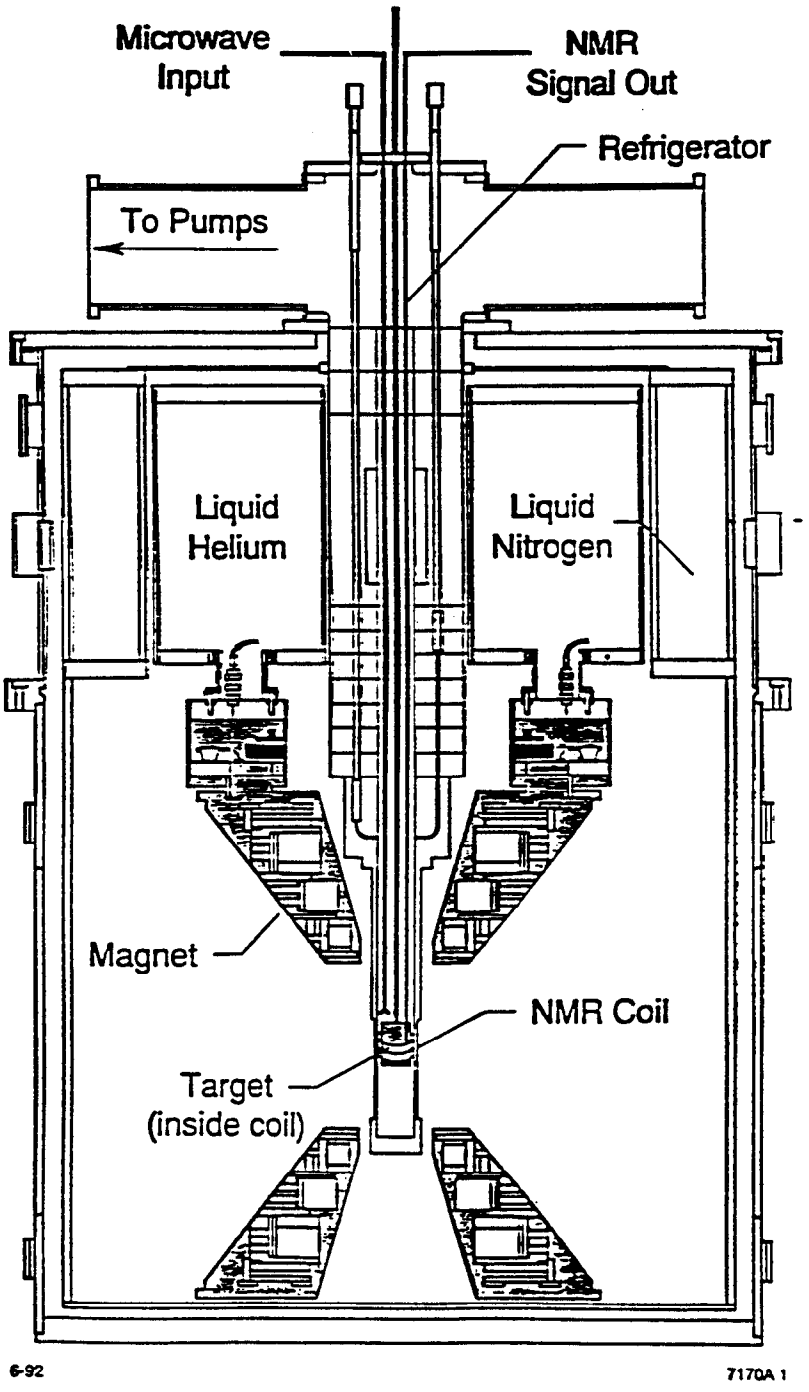

Fig. 11. A sketch of the cryostat and coil for the ammonia target.

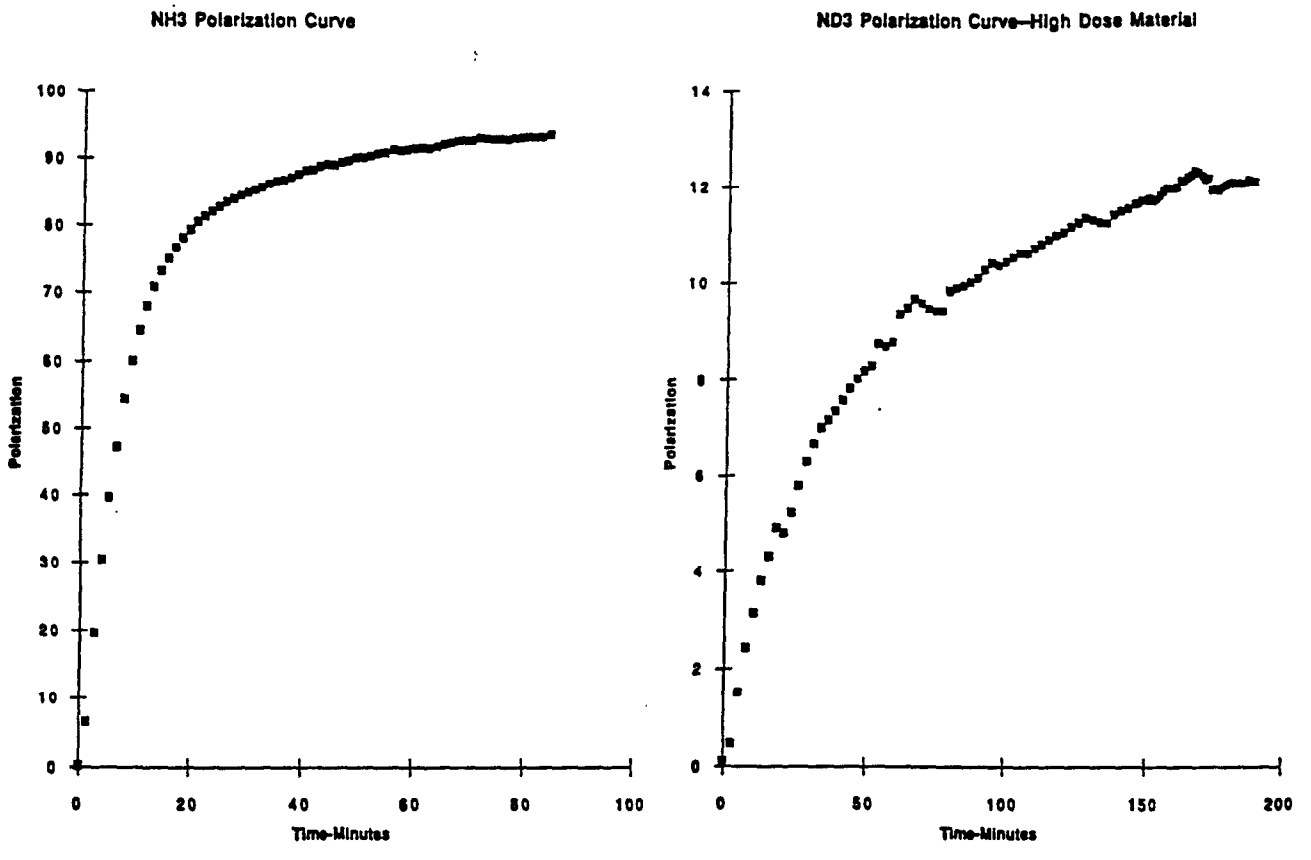

Fig. 12. NH_3 and ND_3 polarization curves obtained during testing at the University of Virginia.

Spectrometers

We propose to assemble two magnetic spectrometers, one on each side of the beam, at central angles of 2.75° and 4.25°, as shown in Figure 13. Each spectrometer is entirely made up of existing ESA magnets, and there are sufficient power supplies to run both dipoles and all five quadrupoles each at their maximum rated power. The design is the same as for the 49 GeV part of proposal E149.

Each spectrometer consists of a quadrupole (or quadrupole doublet), which is followed by a dipole, and another quadrupole in a QDQ design. The quadrupoles are of the Q81 and Q82-type from the 8 GeV/c and 20 GeV/c spectrometers, and the bends are B81 and B82. The dipoles bend the particles down towards the floor, while all the quadrupoles are tuned for vertical focusing and horizontal de-focusing. This is necessary to get an approximate momentum focal plane. The dipoles have in each case been placed as close to the target as possible to achieve large solid angles. The placement of quadrupoles both before and after the dipole allows for the largest possible solid angle consistent with achieving a focus of the vertical scattering angle along the tilted focal plane.

The bending of the dipoles is not very large, but it is sufficient to place the detectors in every case at least 80 cm below a direct line-of-sight of the target. The neutral particles (mostly photons) that hit the pole face of the dipole can "bounce" directly into the detector, so each detector element must be fairly resistent to low energy photons and neutrons.

The QDQ design and small bend angle allows for a relatively flat momentum acceptance over a wide range of momentum. The typical solid angle for the 2.75° spectrometer is 0.3 msr, while for the 4.25° spectrometer it is 0.6 msr. The acceptances of these spectrometers are a factor of 3 larger than those of the spectrometers used in E142/E143, and they operate at twice the momentum. To cover the required E' range the spectrometers will be operated at two settings of the central momentum, a low setting covering E' from 10 to 21 GeV, and a high setting covering 21 to 42 GeV. The momentum dependence of the solid angle for each

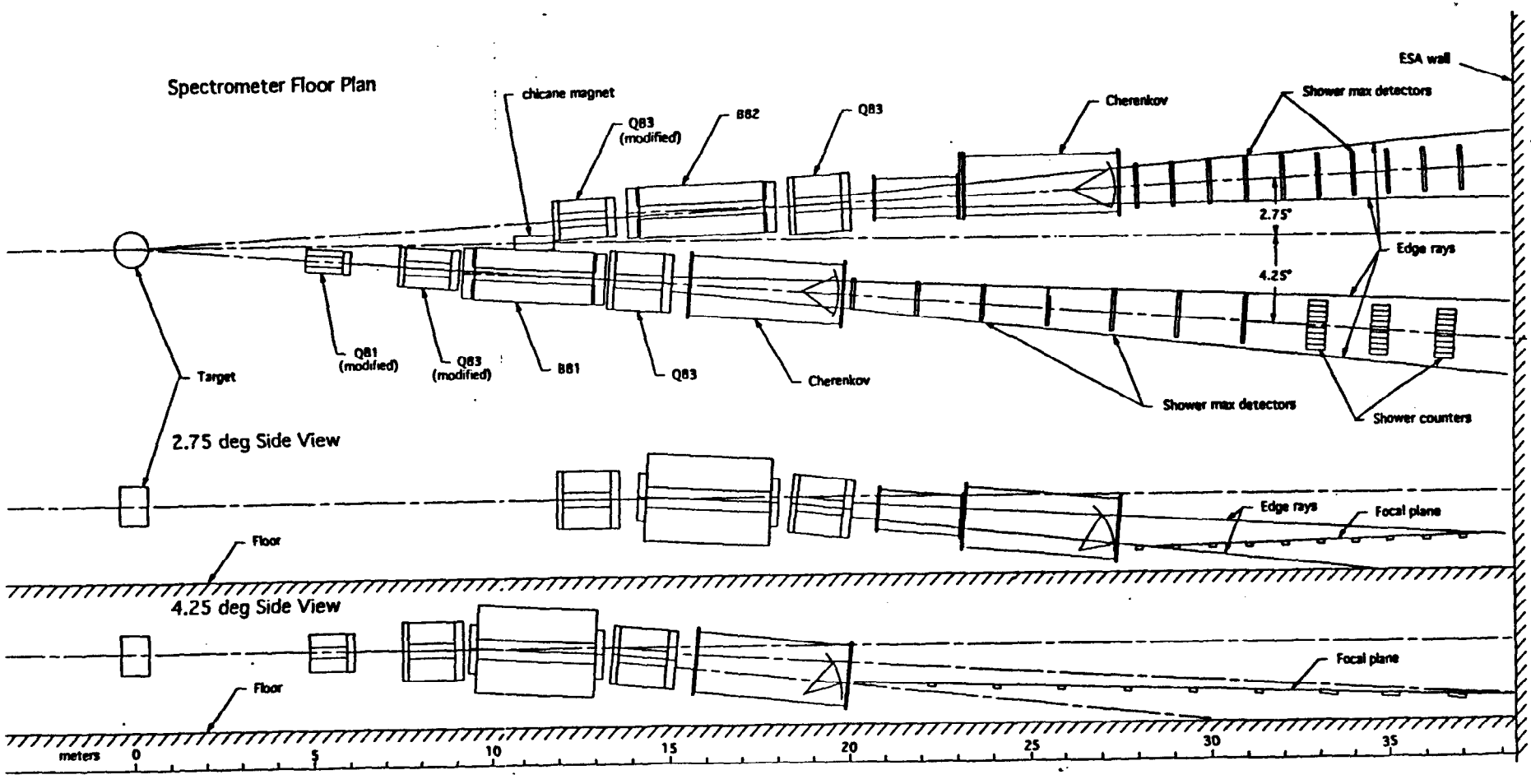

Fig. 13. Proposed spectrometer layout.

spectrometer is shown for the high momentum setting (21 to 42 GeV/c) in Figure 14. For the low momentum settings (10 to 21 GeV/c), all magnets will be run at half their maximum power.

Fig. 14. The acceptance of the two spectrometers as a function of momentum for the high central momentum setting. The acceptance at the low central momentum setting (or any setting) would be the same shape with the momentum values scaled accordingly.

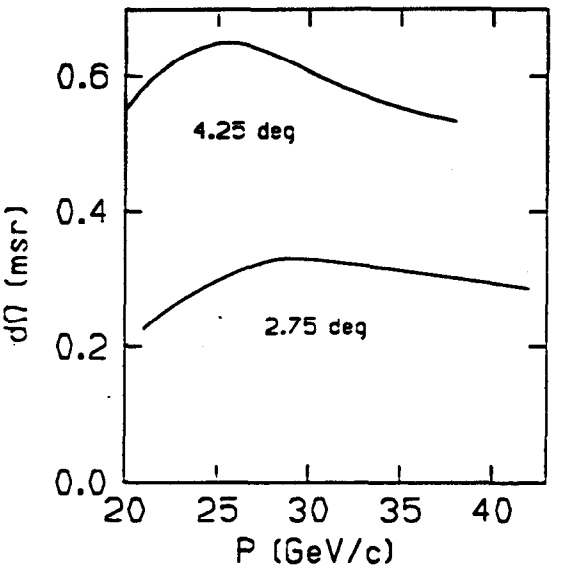

The optics of the spectrometers are shown in Figures 15 and 16. In the horizontal plane the divergence of the rays decreases with increasing momentum, so that shower counters located along the focal plane at various E' will gradually increase in width toward the back. For the essentially point-like target of this experiment, the θ resolution is determined by the size of the detector elements. For detector elements 6 cm wide by 10 cm tall, the θ resolutions are 0.6 mr and 0.9 mr for the 2.75 and 4.25° spectrometers, out of a total acceptance of ±6 and ±9 mr respectively. This is equivalent to resolutions in Q^2 and x of 2.5% and 2.3% respectively. The vertical acceptance is ±15 and ±25 mr for the 2.75 and 4.25° spectrometers respectively. Since this angle is not measured, it contributes an uncertainty in the physics scattering angle of ±5% for both spectrometers, leading to resolutions in x and Q^2 of ±10%. As will be discussed below, if we use 10-cm-tall detectors approximately placed along the tilted focal plane, the momentum resolution for each detector will be better than ±8%, which leads to Q^2 resolutions of ±8%, and

x resolutions which are better than $\pm 10\%$ except at $x > 0.5$, where we plan to use total absorption shower counters to improve the energy resolution. In summary, the total x and Q^2 resolutions of typically $\pm 10\%$ are adequate for the proposed physics, and are well matched to the bin sizes needed for measuring the x and Q^2 dependances of the spin structure functions.

Detectors

The poor duty cycle of the SLED beam (120 nsec pulses at 120 Hz) combined with the high particle rate (up to 20 pions per pulse in the low central momentum setting) and likely high background from single bounce photons in the proposed spectrometers make impractical the use of most tracking detectors, such as wire chambers or scintillator hodoscopes. However, the momentum plane focus makes tracking unnecessary, and only position measurements along the momentum focal plane are needed.

Since the main job of the detectors is to identify electrons with modest position resolution along the focal plane in the presence of up to 35 times higher pion flux, the best type of detectors to use are electromagnetic shower counters, such as lead glass, that have no scintillator in them. We have found that better pion rejection is obtained with thin lead glass blocks located near shower maximum than with thick detectors that sample the entire shower. We call our design "shower-max" detectors. Studies using GEANT have shown that optimal pion rejection is obtained with 6 to 8 r.l. of lead followed by about 2 r.l. of lead glass. At 10 GeV/c and with an electron efficiency of 95%, we expect to achieve a pion rejection of at least 50 to 1 in the shower-max detectors. In this configuration there is an even tradeoff between high lead content glass, such as SF6 (slightly less grams of material for pions to shower in), and lower lead content glass, such as F2 (better light collection, higher threshold against background). Since we have a lot of F2 pieces on hand (about 100 blocks 6 x 6 x 75 cm from the old ASP detector) that can conveniently be cut into 10 cm lengths, we have chosen this option. Following

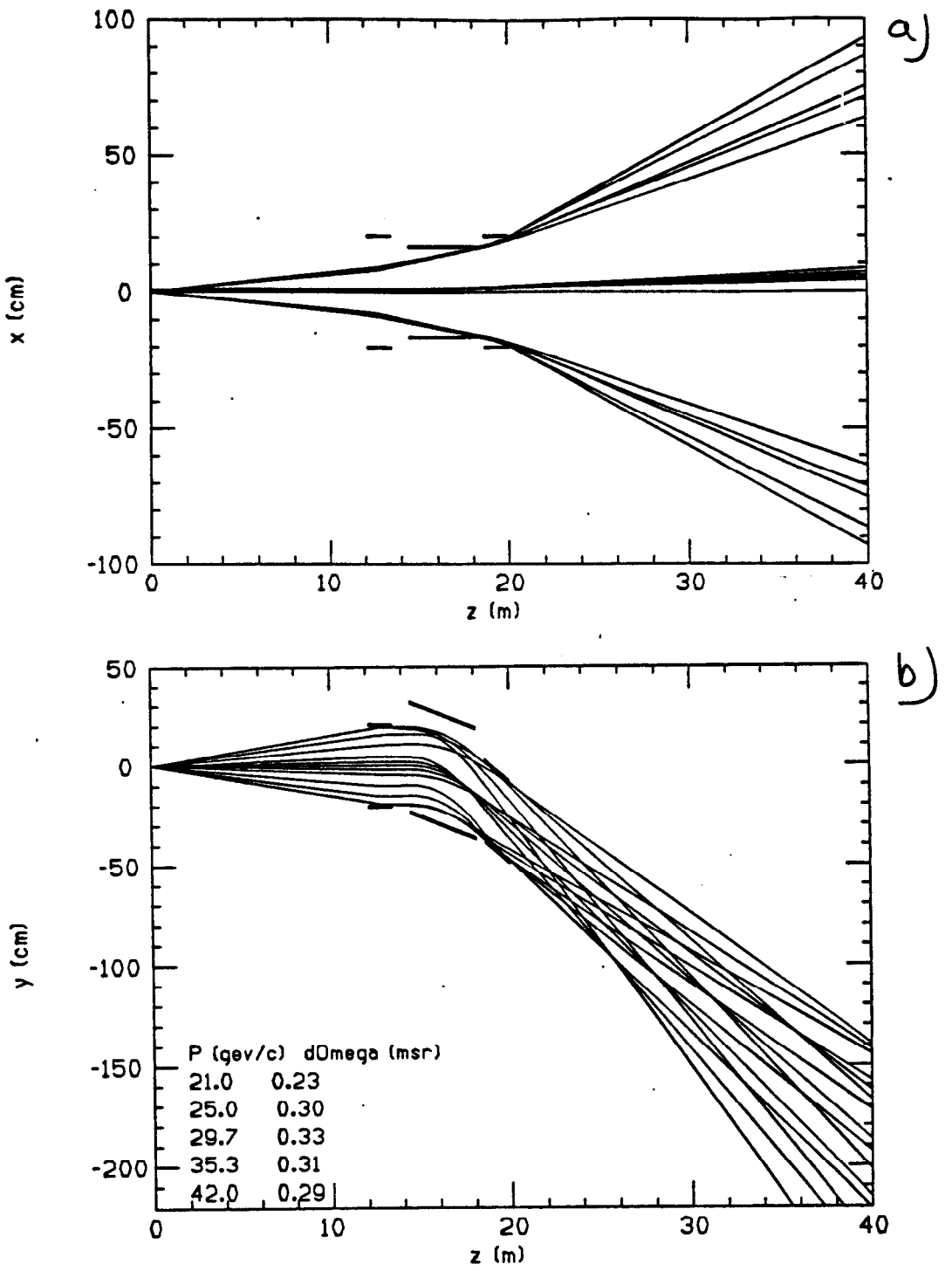

Fig. 15. The optics of the 2.75° spectrometer. Part a) in the non-bend plane, part b) in the bend plane.

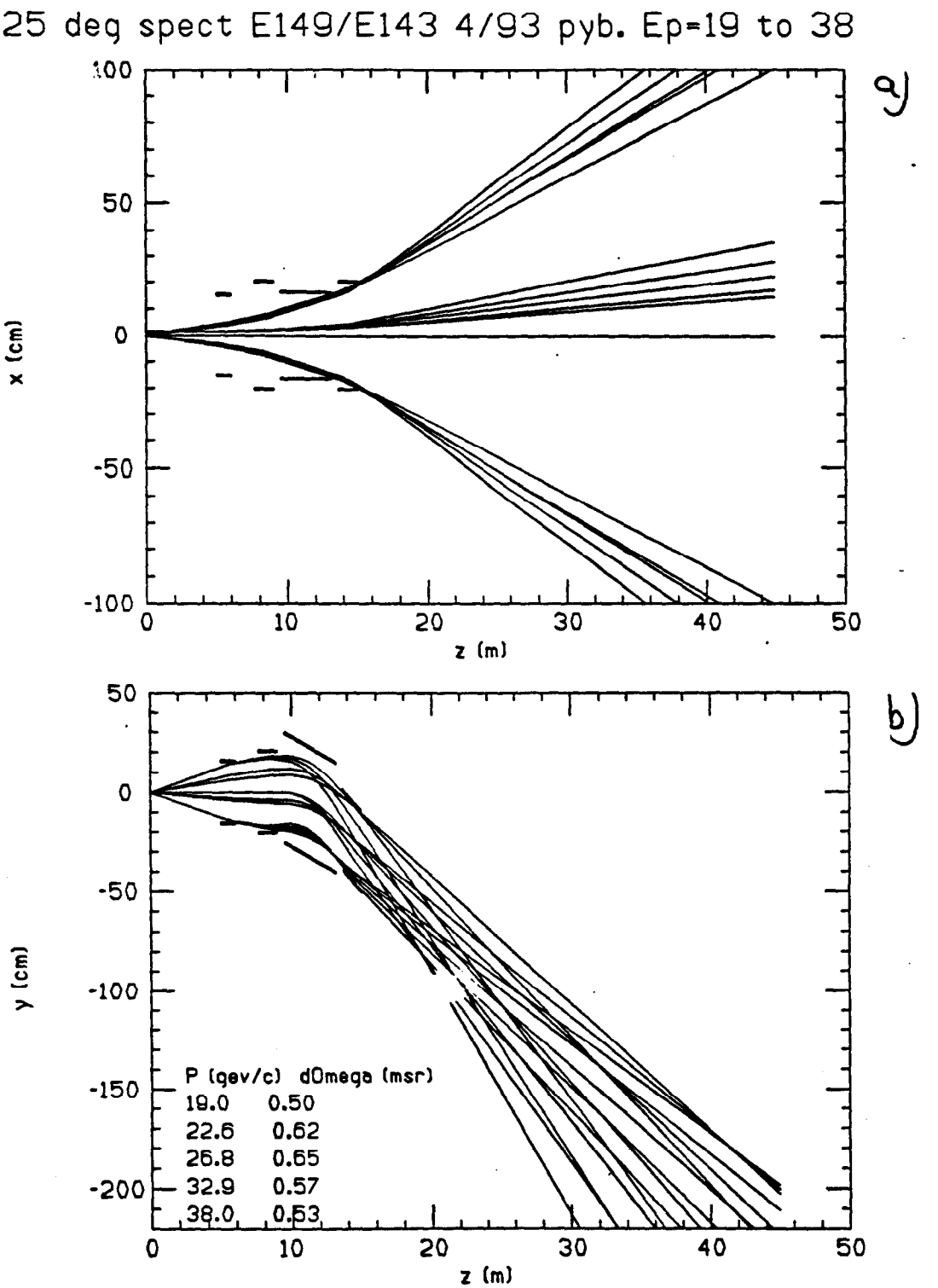

Fig 16. The optics of the 4.25° spectrometer. Part a) in the non-bend plane, part b) in the bend plane.

each piece of lead glass is 30 r.l. of lead or tungsten to completely stop the electron showers. This prevents leakage into the following detectors.

The layout of one of the detector rows is shown in Figure 17. We will need a total of 20 rows (10 per spectrometer), each with from 18 to 22 glass blocks 6 by 6 by 10 cm placed side by side horizontally. This results in a total of $\sim$ 400 pieces of lead glass each with its own phototube. While the lead glass is available, we will need to acquire $\sim$ 400 fast 2-inch photomultiplier tubes.

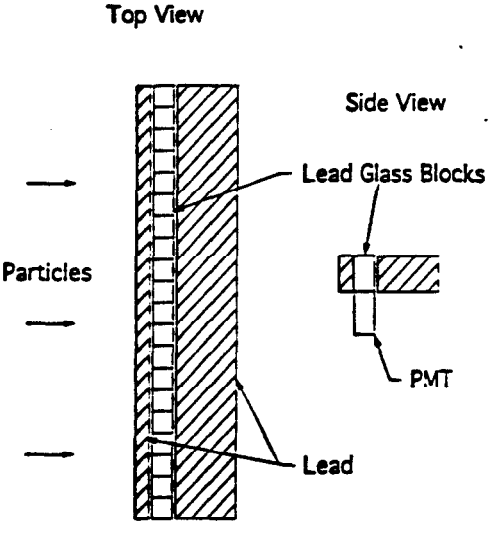

Fig. 17. The layout of a typical row of the shower-max detectors showing the lead filter in front of the row of lead glass blocks, followed by a lead absorber to stop the electromagnetic showers.

For the high momentum setting in the 4.25° spectrometer when measuring high x, the x resolution using the detectors discussed above is not adequate. However, the pion flux at these kinematics is very low, so the optimum pion rejection from the lead glass is not required. To obtain the desired x resolution the top three rows will be total-absorption lead-glass detectors with totally active volumes. A lead-glass preradiator about 3 to 5 r.l. thick, followed by long blocks about 20 r.l. thick can measure the total shower energy with resolution of about $\sigma = \frac{6\%}{\sqrt{E}}$. This would give E' resolutions of 1% at 35 GeV to 40 GeV, which is quite adequate.

Two possible configurations using (mostly) existing lead glass at SLAC are being considered. One would use the 40 existing SF6 blocks (10 x 10 x 25 cm from experiment NE4) to make the back portion of these rows. Another possibility

is to use the 27 SF5 blocks (14.6 x 14.6 x 40 cm) from the 8 GeV spectrometer shower counter for the back portion. In both cases new pre-radiator blocks would be purchased. Further studies will determine the optimum configuration.

Figure 18 shows the distribution of hits in the 10 rows of shower detectors as a function of the incoming particle momentum for the high momentum setting: Part a) the 2.75° spectrometer; part b) the 4.25° spectrometer This figure shows the E' resolution mainly determined by the detector width at low momentum, while for the top two or three bins there is some smearing due to the optics of the spectrometer.

In addition to the lead glass detectors, we plan to use gas Čerenkov detectors to help distinguish pions from electrons. The large 4-m tanks built for E142/E143 showed that good pion rejection could be obtained up to 13 GeV/c with 7 photoelectrons on average per detected electron. For the 4.25° spectrometer we plan to use one 4-m tank and reduce the gas pressure further to raise the pion threshold to 20 GeV/c, while still retaining 3 photoelectrons per electron. This will give adequate electron efficiency (around 95%) and make the detector less sensitive to low energy background. For the 2.75° spectrometer, where the pion rates are the largest at the lowest x, we plan to connect one 2-m tank from E142/E143 together with a 4-m tank for a total of 6-m tank length. At a pion threshold of 20 GeV this should give 4.5 photoelectrons, which is very good. With the Čerenkov detectors we expect to achieve an additional pion rejection power of at least 20:1 for pions below 20 GeV/c. For an initial π/e ratio of 35:1 at our lowest x value of 0.015, the final pion contamination will be quite tolerable at only 0.035. At larger values of x, the pion contamination will drop rapidly (see Figure 9).

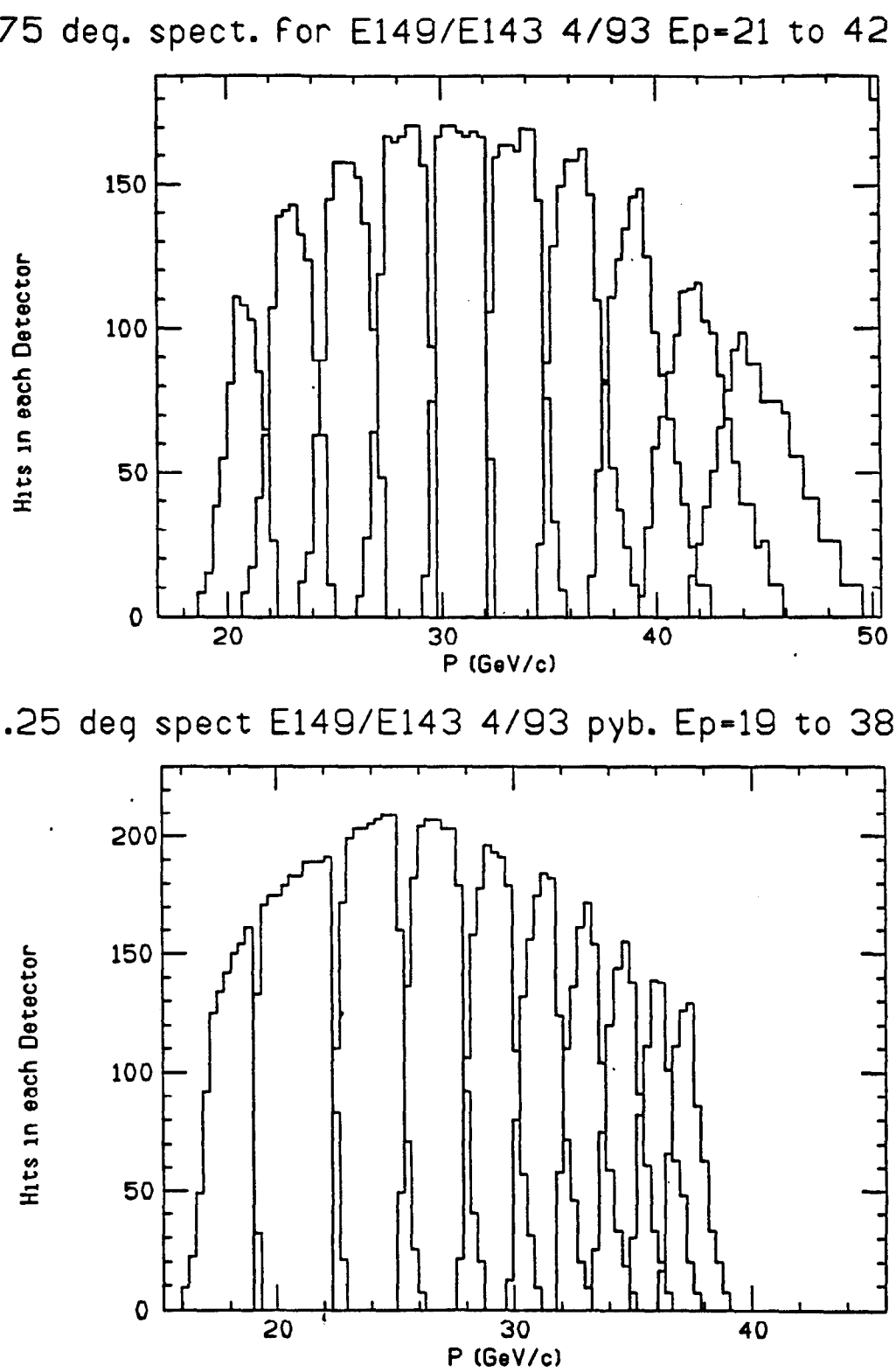

Fig. 18. The distribution of particle hits in the 10 rows of the shower detectors as a function of E'. The envelope follows the shape of the spectrometer acceptance, while the widths of the individual distributions demonstrates the resolution in E'.

Electronics and Data Acquisition

We plan to have one ADC channel for each detector, with a gate width of 150 nsec (essentially the length of the beam pulse), for a total of about 400 channels. We will also have one 16-hit TDC on each channel. Since the ADC gate covers the entire beam pulse, we will not need a lot of electronics to make convention "triggers". All of the required electronics presently exist in End Station A, and sufficient cables exist to carry the signals from the detectors to the counting house. At a rate of 20 pions and 1 electron per spill per spectrometer, the total data rate from all detectors will be less than the 2700 byte per spill data rate of the present data acquisition system. If the data rates from random hits prove too high, we will raise the discriminator thresholds until they are tolerable.

Our present estimate is that the data acquisition system projected to be in place for E143 will be adequate for this experiment. However, experience with E143 may indicate that some modest improvements or upgrades to the system are required.

RUNPLAN AND REQUEST TO THE LABORATORY

Table III

Run Plan and Beam Time Request

Data	Spectrometer Momentum	Hours
NH3 Parallel	low E'	100
	high E'	100
ND3 Parallel	low E'	160
	high E'	160
NH3 Perpendicular	low E'	20
	high E'	20
ND3 Perpendicular	low E'	20
	high E'	20
Calibration and normalization to E143		30
σ at low x		40
Positron and empty target		10
Total hours at 100% efficiency		680
Overhead (target anealing, beam polarization, target spin rotataion)	(×1.6)	1088
Loboratory efficiency	(×2)	2176
Total beam time request		three calendar months
Parasitic A-line beam for checkout and calibration		six weeks

APPENDIX

Kinematics and Structure Function Formulas

The experimental quantities used to determine the spin structure functions are the two asymmetries:

$$A^{\parallel} = \frac{\sigma^{\uparrow\downarrow} - \sigma^{\uparrow\uparrow}}{\sigma^{\uparrow\downarrow} + \sigma^{\uparrow\uparrow}} \quad \text{and} \quad \mathrm{A}^{\perp} = \frac{\sigma^{\downarrow\leftarrow} - \sigma^{\uparrow\leftarrow}}{\sigma^{\downarrow\leftarrow} + \sigma^{\uparrow\leftarrow}}. \tag{14}$$

Here $\sigma^{\uparrow\downarrow}(\sigma^{\uparrow\uparrow})$ is defined in Eq. (2), and $\sigma^{\downarrow\leftarrow}(\sigma^{\uparrow\leftarrow})$ is defined in Eq. (3). The experimental asymmetries $A^{\parallel}$ and $A^{\perp}$ are related to the virtual photon-nucleon longitudinal and transverse asymmetries A_1 and A_2,

$$A_1 = \frac{\sigma_{1/2} - \sigma_{3/2}}{\sigma_{1/2} + \sigma_{3/2}}, \quad \text{and} \quad \mathrm{A}_2 = \frac{\sigma_{\mathrm{TL}}}{\sigma_{\mathrm{T}}}.$$

$$A^{\parallel} = D(A_1 + \eta A_2) \ \text{ and } \ A^{\perp} = d(\zeta A_1 - A_2), \tag{15}$$

where

$$D = (1 - E'\epsilon/E)/(1 + \epsilon R), \tag{16}$$

$$\eta = (\epsilon\sqrt{Q^2}/(E - E'\epsilon), \tag{17}$$

$$d = D\sqrt{(2\epsilon/(1+\epsilon)}, \tag{18}$$

$$\zeta = \eta((1+\epsilon)/2\epsilon), \tag{19}$$

$$1/\epsilon = 1 + 2[1 + (\nu^2/Q^2)]\tan^2(\theta/2). \tag{20}$$

Here $\sigma_{1/2}(\sigma_{3/2})$ is the virtual photoabsorption cross section when the projection of the total angular momentum of the photon-nucleon system along the incident

lepton direction is $\frac{1}{2}(\frac{3}{2})$, and $\sigma_T = \frac{1}{2}(\sigma_{1/2} + \sigma_{3/2})$ is the total transverse photoabosrption cross section, and σ_{TL} is a term arising from the interference between transverse and longitudinal amplitudes. The factor $R = \sigma_L/\sigma_T$ is the ratio of longitudinal to transverse virtual photoabsorption cross-sections. The factor D is the virtual photon depolarization.

The virtual photon asymmetries A_1 and A_2 can in turn be expressed in terms of the measured $A^{\parallel}$ and $A^{\perp}$ as

$$A_1 = \frac{A^{\parallel}}{D[1+\zeta\eta]} - \frac{\eta A^{\perp}}{d[1+\zeta\eta]} \tag{21}$$

$$A_2 = \frac{\zeta A^{\parallel}}{D[1+\zeta\eta]} + \frac{A^{\perp}}{d[1+\zeta\eta]} \tag{22}$$

The asymmetries A_1 and A_2 can also be expressed in terms of the structure functions g_1 and g_2 as

$$A_1 = (g_1 - \gamma^2 g_2)\frac{1}{F_1} \quad \text{and} \quad A_2 = \gamma(g_1 + g_2)\frac{1}{F_1}, \tag{23}$$

where $\gamma = \sqrt{Q^2}/\nu$ and F_1 is the spin independent structure function.

Solving Equation (23) for g_1 and g_2

$$g_1 = \frac{F_1[A_1 + \gamma A_2]}{1+\gamma^2} \quad \text{and} \quad g_2 = \frac{F_1[\frac{1}{\gamma}A_2 - A_1]}{1+\gamma^2}. \tag{24}$$

In previous work where transverse asymmetries were not measured it has been customary to ignore the term containing A_2. Since γ and η are small at sufficiently large Q^2 in the kinematic range of the experiments, the approximation is made that

$$A_1 \simeq A^{\parallel}/D, \tag{25}$$

and then

$$g_1 \simeq A_1 F_1 = A_1 F_2/2x(1+R). \tag{26}$$

where F_2 is the second spin independent structure function. This is the method

used by EMC and SMC.

When transverse asymmetries are measured but the cross section σ is not measured, then the A_2 terms are included, but the factor R in the virtual photon depolarization needed to extract A_1 and A_2 from the measured $A^{\parallel}$ and $A^{\perp}$ must be determined from cross sections measured in other experiments or from models. This was the method used by E142 where the neutron spin structure function was extracted via $g_1^n = (A_1^n F_1^n + \gamma A_2^n F_1^n)/(1+\gamma^2)$. Here F_1^n is the spin averaged structure function of the neutron.

The experimental method proposed in this experiment will measure $A^{\parallel}$ and $A^{\perp}$ and the unpolarized cross section σ. The spin structure functions g_1 and g_2 will then be extracted directly from the measured quantities using the expressions[11]

$$g_1(x) - k g_2(x) = 2K A^{\parallel} \sigma / \sigma_{Mott}, \tag{27}$$

$$g_1(x) + k' g_2(x) = 2K' A^{\perp} \sigma / \sigma_{Mott}, \tag{28}$$

where the Mott cross section is

$$\sigma_{Mott} = 4\alpha^2 E'^2 \cos^2(\theta/2)/Q^4, \tag{29}$$

and the kinematical factors are defined by

$$K = EE' \cos^2(\theta/2)/[2x(E + E'\cos\theta)] \quad \text{and} \quad k = 2xM/(E + E'\cos\theta). \tag{30}$$

$$K' = E\cos^2(\theta/2)/(2x\sin\theta) \quad \text{and} \quad k' = 2E/(E - E'). \tag{31}$$

Factors and Assumptions Used in Estimating Kinematics, Counting Rates, and Experimental Errors

Assumptions for calculations

1. Beam current = 2.0×10^9 electrons/pulse.
2. Beam polarization = 80%.
3. Target density (NH3) = 0.87 g/cm^3.
4. Target density (ND3) = 1.04 g/cm^3.
5. Helium density = 0.125 g/cm^3.
6. Target length = 3.0 cm.
7. % ammonia in target = 60.0%.
8. % helium in target = 40.0%.
9. Amount of additional helium = 0.4 cm
10. ^{15}NH3 proton polarization = 90%.
11. ^{15}ND3 deuterium polarization = 40%.
12. ^{15}NH3 mass = 18.024 g/mole.
13. ^{15}ND3 mass = 21.042 g/mole.
14. ^{4}He mass = 4.003 g/mole.
15. 100 hours of data at 100% efficiency at each of two spectrometer central momenta for NH3.
16. 160 hours of data at 100% efficiency at each of two spectrometer central momenta for ND3.
17. Spectrometer solid angles versus E' as shown in Figure 14.

Kinematics

1. Beam energy = 48.55 GeV.

2. Small angle spectrometer $\theta_1 = 2.75 \pm 0.34$ degrees.
3. Large angle spectrometer $\theta_2 = 4.25 \pm 0.57$ degrees. The θ acceptances are used in the Q^2 related calculations.

Notes

1. Minimum x attainable was based on π/e cut at 40 and $Q^2 > 1.0$.
2. Maximum x attainable was based on missing mass requirement $W^2 > 4$ to stay away from the resonance region.
3. Whitlow models[29] were used for F_2 and R.
4. Assumed $g_2 = 0$.
5. Pion rates were calculated via the WISER code[30] using a total of 6% radiator thickness.
6. 1.5% correction for nitrogen polarization was applied.
7. For E143 comparisons:
   (a) Beam energy = 25.9 GeV.
   (b) Small angle spectrometer $\theta_1 = 4.5 \pm 0.26$ degrees.
   (c) Large angle spectrometer $\theta_2 = 7.0 \pm 0.69$ degrees.
8. Proton asymmetry model[6] used:

$$A_1^p = 1.025x^{0.12}[1.0 - \exp^{-2.7x}]$$

9. Neutron asymmetry model[31] used:

$$A_1^n = 3.599x^{1.4}(1.0 - x) + x(3.648x - 2.665)$$

In the following table(s):
DEPOL is the depolarization factor.
RC is the applied rad. cor. factor which divides the born cross sections to give raw cross sections
PI/E is the expected pion/electron rate ratio.
EL/SPILL is the total expected electron counting rate per spill for the given x bin.
F is the dilution factor.
ERROR is the error on the measured asymmetry/DEPOL for 100 hours of running (PROTON) and 160 hours of running (DEUTERON).

E0 = 48.560; THETA = 2.75; SPECTROMETER TYPE = 3

									******** PROTON ********			******* DEUTERON *******		
EP	NU	Q2	W	X		RC	DEPOL	PI/E	EL/SPILL	F	ERROR	EL/SPILL	F	ERROR
10.458	38.102	1.170	8.439	0.016	*	0.38	0.7986	32.2181	0.1280	0.155	0.005	0.1489	0.259	0.005
11.392	37.168	1.274	8.328	0.018	*	0.41	0.7773	26.6963	0.1424	0.155	0.005	0.1657	0.259	0.005
12.382	36.178	1.385	8.209	0.020	*	0.44	0.7546	21.4118	0.1575	0.155	0.004	0.1832	0.259	0.004
13.428	35.132	1.502	8.081	0.023	*	0.47	0.7306	16.6266	0.1624	0.155	0.005	0.1890	0.259	0.005
14.526	34.034	1.625	7.945	0.025	*	0.50	0.7053	12.5066	0.1666	0.155	0.005	0.1938	0.259	0.005
15.674	32.886	1.753	7.800	0.028	*	0.52	0.6789	9.1196	0.1631	0.155	0.005	0.1896	0.259	0.005
16.868	31.692	1.886	7.646	0.032	*	0.55	0.6514	6.4526	0.1566	0.156	0.005	0.1821	0.259	0.005
18.102	30.458	2.025	7.484	0.035	*	0.58	0.6230	4.4354	0.1502	0.156	0.006	0.1746	0.259	0.005
19.372	29.188	2.167	7.313	0.040	*	0.61	0.5938	2.9662	0.1436	0.156	0.006	0.1670	0.259	0.006
SPECTROMETER TOTAL								14.3540	1.3704			1.5938		

E0 = 48.560; THETA = 2.75; SPECTROMETER TYPE = 3

									******** PROTON ********			******* DEUTERON *******		
EP	NU	Q2	W	X		RC	DEPOL	PI/E	EL/SPILL	F	ERROR	EL/SPILL	F	ERROR
21.317	27.243	2.384	7.044	0.047	*	0.65	0.5492	1.5523	0.2083	0.156	0.005	0.2421	0.259	0.005
23.863	24.697	2.669	6.675	0.058	*	0.70	0.4916	0.6294	0.2444	0.157	0.005	0.2837	0.259	0.005
26.417	22.143	2.954	6.283	0.071	*	0.76	0.4354	0.2384	0.2649	0.158	0.006	0.3073	0.259	0.006
28.925	19.635	3.235	5.873	0.088		0.81	0.3825	0.0858	0.2724	0.159	0.007	0.3157	0.259	0.007
31.334	17.226	3.504	5.450	0.108		0.86	0.3344	0.0299	0.2637	0.160	0.008	0.3051	0.259	0.008
33.601	14.959	3.758	5.019	0.134		0.92	0.2906	0.0102	0.2471	0.162	0.009	0.2853	0.259	0.009
35.691	12.869	3.992	4.587	0.165		0.97	0.2507	0.0035	0.2285	0.165	0.011	0.2632	0.260	0.011
37.585	10.975	4.203	4.156	0.204		1.03	0.2142	0.0012	0.2071	0.168	0.013	0.2377	0.260	0.014
39.273	9.287	4.392	3.730	0.252		1.08	0.1814	0.0004	0.1825	0.172	0.016	0.2086	0.260	0.017
SPECTROMETER TOTAL								0.2715	2.1190			2.4486		

E0 = 48.560; THETA = 4.25; SPECTROMETER TYPE = 4

									******** PROTON ********			******* DEUTERON *******		
EP	NU	Q2	W	X		RC	DEPOL	PI/E	EL/SPILL	F	ERROR	EL/SPILL	F	ERROR
10.903	37.657	2.911	8.285	0.041	*	0.48	0.7987	35.5649	0.0538	0.156	0.007	0.0625	0.259	0.007
11.808	36.752	3.153	8.167	0.046	*	0.51	0.7797	25.8380	0.0544	0.157	0.007	0.0632	0.259	0.007
12.762	35.798	3.408	8.040	0.051	*	0.54	0.7596	18.1062	0.0533	0.157	0.008	0.0619	0.259	0.008
13.765	34.795	3.676	7.906	0.056	*	0.57	0.7389	12.2406	0.0514	0.157	0.008	0.0596	0.259	0.008
14.814	33.746	3.956	7.762	0.062	*	0.60	0.7179	7.9877	0.0478	0.158	0.008	0.0554	0.259	0.008
15.907	32.653	4.248	7.610	0.069	*	0.63	0.6968	5.0367	0.0443	0.158	0.009	0.0514	0.259	0.009
17.040	31.520	4.550	7.448	0.077	*	0.67	0.6754	3.0736	0.0414	0.159	0.010	0.0480	0.259	0.010
18.208	30.352	4.862	7.278	0.085	*	0.70	0.6536	1.8187	0.0390	0.159	0.010	0.0452	0.259	0.010
19.407	29.153	5.182	7.100	0.095	*	0.73	0.6309	1.0456	0.0366	0.160	0.011	0.0423	0.259	0.011
SPECTROMETER TOTAL								13.6359	0.4220			0.4896		

E0 = 48.560; THETA = 4.25; SPECTROMETER TYPE = 4

									******** PROTON ********			******* DEUTERON *******		
EP	NU	Q2	W	X		RC	DEPOL	PI/E	EL/SPILL	F	ERROR	EL/SPILL	F	ERROR
21.317	27.243	5.693	6.805	0.111	*	0.78	0.5938	0.4202	0.0777	0.161	0.008	0.0899	0.259	0.008
23.863	24.697	6.372	6.392	0.137	*	0.84	0.5421	0.1179	0.0786	0.163	0.008	0.0907	0.259	0.009
26.417	22.143	7.055	5.948	0.170	*	0.91	0.4878	0.0308	0.0741	0.166	0.009	0.0853	0.260	0.010
28.925	19.635	7.724	5.477	0.210		0.97	0.4326	0.0077	0.0645	0.169	0.011	0.0739	0.260	0.012
31.334	17.226	8.368	4.984	0.259		1.03	0.3782	0.0019	0.0538	0.173	0.014	0.0614	0.260	0.015
33.601	14.959	8.973	4.470	0.320		1.10	0.3263	0.0005	0.0429	0.178	0.017	0.0487	0.261	0.020
35.691	12.869	9.531	3.937	0.395		1.16	0.2782	0.0001	0.0319	0.185	0.023	0.0359	0.261	0.027
37.585	10.975	10.037	3.382	0.487		1.22	0.2349	0.0000	0.0204	0.192	0.032	0.0228	0.262	0.040
39.273	9.287	10.488	2.797	0.602		1.29	0.1967	0.0000	0.0102	0.199	0.053	0.0113	0.263	0.067
SPECTROMETER TOTAL								0.0987	0.4542			0.5199		

REFERENCES

1. J.D. Bjorken, *Phys. Rev.* **148**(1966), 1467, *Phys.Rev.* **D1**(1970), 1376
2. J. Ellis and R.L. Jaffe, *Phys.Rev.* **D9**(1974), 1444, **D10**(1974), 1669
3. SMC, CERN/SPSC 88-47 (1988).
4. SMC, CERN-PPE/93-47 (1993), submitted to Phys. Lett. B
5. P. L. Anthony, *et al.*, SLAC-PUB-6101, (1993), submitted to Phys. Rev. Lett.
6. The EMC collaboration, J. Ashman *et al.*, *Nucl.Phys.* **B328**(1989), 1
7. M.J. Alguard *et al.*, *Phys.Rev.Lett.* **37**(1976), 1261 , *Phys.Rev.Lett* **41**(1978), 70
8. G. Baum *et al.*, *Phys.Rev.Lett* **51**(1983), 1135
9. C.E. Carlson and Wu-Ki Tung,, *Phys.Rev.* **D5**(1972), 721
10. A.J.G. Hey and J.E. Mandula,, *Phys.Rev.* **D5**(1972), 2610
11. E. Leader and M. Anselmino, *Z.Phys.* **C41**(1988), 239
12. R. L. Jaffe and A. Manohar, *Nucl.Phys.* **B337**(1990), 509
13. H. Burkhardt and W.N. Cottingham, *Ann.Phys(N.Y.)* **56**(1970), 453
14. W. Wandzura and F. Wilczek, *Phys.Lett* **B172**(1977), 195
15. V.M. Belyaev and B.L. Ioffe, *Int.J.Mod.Phys* **A6**(1991), 1533
16. R.L. Heimann, *Nucl.Phys.* **B64**(1973), 429
17. R.L. Jaffe and Xiangdong Ji, *Phys.Rev.* **D43**(1991), 726
18. M. Virchaux, A. Milsztajn,, *Phys. Letters* **B274**(1992), 221
19. M.L. Seely *et al.*, *Nucl.Inst.Meth.* **201**(1982), 303
20. D.G. Crabb *et al.*, *Phys.Rev.Lett* **64**(1990), 2627
21. T.O. Niinikoski and J. M. Rieubland, *Phys.Lett.* **A72**(1979), 141

22. W.W. Ash, Proc. High Energy Physics with Polarized Beams and Targets, Ed. M.L. Marshak (AIP New York 1976) P. 485

23. U. Haertel *et al.* , High Energy Physics with Polarized Beams and Polarized Targets, eds., C. Joseph and J. Soffer, Birkhauser Verlag, Basel (1981) p. 447

24. D.G. Crabb *et al.* , Proc. 4th. Intl. Workshop on Polarized Target Materials and Techniques, Bonn 1984, Ed. W. Meyer, P. 7

25. W. Meyer *et al.*, *Nucl.Instr.Meth.* **215**(1983), 65

26. D.G. Crabb, Proc. High Energy Spin Physics, Bonn 1990, Eds. W. Meyer, E. Steffens, W. Thiel, Springer Verlag 1991, P. 289

27. M. L. Seely et al., Proc. Int. Conf. on High Energy Spin Physics, Brookhaven 1982, ed. G. Bunce, AIP Conf. Proc. 95(1982), 526

28. K. H. Althoff et. al., 4th Intl. Workshop on Polarized target Materials and Techniques, Bonn 1984, Ed. W. Meyer, p. 25.

29. L. W. Whitlow, Ph.D. thesis, Stanford University SLAC-Report-357 (March 1990)

30. D. Wiser, Ph.D Thesis, University of Wisconsin (1977)

31. Private communication from the E142 collaboration.